A newly developed APCC SCoPS and its prediction of East Asia seasonal climate variability

Suryun Ham[1*], A-Young Lim[1], Suchul Kang[2], Hyein Jeong[3], and Yeomin Jeong[1], Bin Wang[4,5], Baoqiang Xiang[6,7], Shu Wu[8], Joshua-Xiouhua Fu[9,10]

[1]Climate Services and Research Department, APEC Climate Center, Korea
[2]Ralph M. Parsons Laboratory, Massachusetts Institute of Technology, USA
[3]Fluid Dynamics and Solid Mechanics (T-3), Theoretical Division, Los Alamos National Laboratory, USA
[4]Department of Atmospheric Sciences and International Pacific Research Center, School of Ocean and Earth Science and Technology, University of Hawaii, Hawaii, USA
[5]Earth System Modeling Center, Nanjing University of Information Science and Technology, Nanjing, China
[6]NOAA/Geophysical Fluid Dynamics Laboratory, Princeton, New Jersey
[7]University Corporation for Atmospheric Research, Boulder, Colorado, USA
[8]Nelson Institute Center for Climatic Research, University of Wisconsin-Madison, WI, USA
[9]International Pacific Research Center, School of Ocean and Earth Science and Technology, University of Hawaii, Hawaii, USA
[10]Department of Atmospheric and Oceanic Sciences, FuDan University, Shanghai, China

(To be submitted Climate Dynamics)

*Corresponding author address:
Suryun Ham, Climate Services and Research Department,
APEC Climate Center, Busan, 48058, Korea
E-mail: suryun01@gmail.com

Abstract

The Asia Pacific Economic Cooperation (APEC) Climate Center (APCC) in-house model (Seamless Coupled Prediction System: SCoPS) has been newly developed for operational seasonal forecasting. SCoPS has generated ensemble retrospective forecasts for the period 1982–2013 and real-time forecasts for the period 2014–current. In this study, the seasonal prediction skill of the SCoPS hindcast ensemble was validated compared to those of the previous operation model (APEC Climate Center Community Climate System Model version 3: APCC CCSM3). This study validated the spatial and temporal prediction skills of hindcast climatology, large-scale features, and the seasonal climate variability from both systems. A special focus was the fidelity of the systems to reproduce and forecast phenomena that are closely related to the East Asian monsoon system. Overall, both CCSM3 and SCoPS exhibit realistic representations of the basic climate, although systematic biases are found for surface temperature and precipitation. The averaged temporal anomaly correlation coefficient for sea surface temperature, 2-m temperature, and precipitation from SCoPS is higher than those from CCSM3. Notably, SCoPS well captures the northward migrated rainband related to the East Asian summer monsoon. The SCoPS simulation also shows useful skill in predicting the wintertime Arctic Oscillation. Consequently, SCoPS is more skillful than CCSM3 in predicting seasonal climate variability, including the ENSO and the Arctic Oscillation. Further, it is clear that the seasonal climate forecast with SCoPS will be useful for simulating the East Asian monsoon system.

Key words: APCC in-house model, SCoPS, Seasonal prediction, East Asian monsoon

1. Introduction

It has been demonstrated that a fully coupled general circulation model is the ultimate tool for subseasonal to seasonal climate prediction. Dynamical prediction systems have been continuously progressed for operational medium-range weather and seasonal prediction (e.g., Molteni et al. 1996; Kusunoki et al. 2001; Saha et al. 2006, 2014; Arribas et al. 2011; Molteni et al. 2011; MacLachlan et al. 2015; Lee et al. 2014). These dynamical prediction models in operational centers are almost fully coupled climate system models that include comprehensive dynamics and physics of the atmosphere, land surface, ocean, and sea ice interactions. Many studies have demonstrated the importance of model resolution and atmospheric physics as well as the model system on various simulated climate variations. For example, Yao et al. (2016) suggested that coupled model results with higher resolution lead to improved prediction skill on produced climate variations over the western equatorial Indian Ocean. Ham et al. (2014) investigated the effects of an improved coupled system on the simulated seasonal climate over East Asia.

For this reason, operational coupled seasonal forecast systems, including the Climate Forecast System from the National Centers for Environmental Prediction (NCEP CFS) (Saha et al. 2014), European Centre for Medium-Range Weather Forecasts (ECMWF), United Kingdom Meteorological Office (UKMO), and Meteo-France (MacLachlan et al. 2015), as well as many other research groups, are continuously updating their seasonal prediction systems with improved physics and increased resolution. The horizontal resolution of the ECMWF Integrated Forecast System has increased from T159 (System 3; Anderson et al. 2007) to T255 (System 4; Molteni et al. 2011) (from approximately 125 km to 80 km) with model version updating. The UKMO has also increased the atmospheric resolution of the seasonal prediction system to N216L85 (approximately 60 km) in Global Seasonal Forecasting System version 5 (GloSea5) (MacLachlan et al. 2015).

A number of studies mentioned the importance of initialization processes for the prediction skill in the coupled system. For example, Kug et al. (2010) have developed a new method that conducting empirical singular vectors for initial perturbation in an ensemble prediction system. Ham and Rienecker (2012) suggested an improvement in the El Niño-Southern Oscillation (ENSO) prediction using the ensemble generation method in their 20-year reforecast simulation. Koster et al. (2010) mentioned that there is room for improvement in prediction skills for precipitation and surface temperature in land surface initialization. Recently, the importance of initializations of land surface or sea ice content is noted at sub-seasonal to seasonal scales. Prodhomme et al. (2016) showed that realistic initialization of land surface plays a role of improved prediction skill. Dirkson et al. (2017) suggested that accurate initialization of sea ice thickness can improve the seasonal prediction skill for Arctic sea ice area and concentration.

Since 2007, the Asia-Pacific Economic Cooperation (APEC) Climate Center (APCC) has issued global temperature and precipitation prediction information for every following 3–6 month period via the website (http://www.apcc21.org). These deterministic and probabilistic forecasts have been produced by the well-validated multi-model ensemble (MME) prediction (Min et al. 2014). Since 2012, the APCC has provided seasonal prediction data as one provider to the MME prediction system using the Community Climate System Model version 3 (CCSM3) with sea surface temperature (SST) nudging from the Global Ocean Data Assimilation System (GODAS) (APCC CCSM3; Jeong et al. 2008). Recently, the prediction skill of CCSM3 has met the limitations of the old version of the model system with low resolution and simple initialization. To enhance the quality and application of climate forecast information, the APCC has developed an in-house prediction model with a research group from the University of Hawaii, USA. The newly developed high-resolution climate prediction model, termed the Seamless Coupled Prediction System (SCoPS), is a fully coupled ocean, atmosphere, land, and sea ice component model with coupled atmosphere-ocean initialization.

Since various validations on historical reforecasts (i.e., hindcast) can provide a useful guideline for understanding its characteristic, it is very important to further improve the prediction system. In this paper, the newly developed seasonal prediction model (SCoPS) is described and evaluated alongside previous operation model (APCC CCSM3) with a basic validation of the prediction system to reproduce the seasonal climate variability. We also present analysis of the performance of SCoPS for the East Asian monsoon system. The paper is divided into the following sections: a brief description of the APCC CCSM3 and SCoPS framework for hindcast experiments is provided in section 2; section 3 examines hindcast climatology and prediction skills, which are closely related to the East Asian climate; and section 4 summarizes the results and provides major conclusions.

2. Model description

a. APCC CCSM3

CCSM3 has been designed to produce simulations with reasonable fidelity over a wide range of resolutions and with a variety of atmospheric dynamical frameworks. It is a community model system for climate simulation, which includes the Community

Atmosphere Model version 3 (CAM3; Collins et al. 2004, 2006), the Community Land Surface Model version 3 (CLM3; Oleson et al. 2004; Dickinson et al. 2006), and the Community Sea Ice Model version 5 (CSIM5; Briegleb et al. 2004). The ocean component is based on the Parallel Ocean Program (POP) version 1.4.3 (Smith and Gent 2002). Based on generally realistic initial conditions, SST-nudging, an empirical method for data assimilation, is used for initialization in APCC. Further information on the APCC CCSM3 is given in Collins et al. (2006), Jeong et al. (2008), and Kim et el. (2017).

b. SCoPS

The International Pacific Research Center (IPRC) and University of Hawaii (UH) modeling group have developed a new coupled atmosphere-ocean model (POEM) which is based on the POP v2.0 model for the oceanic component, the Ocean-Atmosphere-Sea Ice-Soil (OASIS v3.0) coupler, and the ECMWF-Hamburg Atmospheric Model (ECHAM v4.6) as the atmospheric component (Xiang et al. 2012). A research group at University of Hawaii developed the original version of the in-house prediction model for APCC under the “Agreement between the APEC Climate center and the University of Hawaii on the APCC international research project for development of APCC seamless prediction system”. Based on the POEM system, SCoPS has been newly developed as a fully coupled climate model for seamless prediction of weather and climate (APCC project report 2015). SCoPS consists of the ECHAM version 5.3 (Roeckner et al. 2003, Hagemann et al. 2006) and the Sea Ice Model version 4.1 (Hunk and Lipscomb 2010). The ocean component is based on the Parallel Ocean Program (POP) version 1.4.3 (Smith and Gent 2002). Compared with the

POEM model (Xiang et al. 2012) as well as the previous operational model, APCC CCSM3, SCoPS has some distinct improvements: a newly developed coupled atmosphere-ocean initialization, implanting a sea ice model, updated model physics and coupler versions, and an increase in the atmosphere and ocean model resolutions.

Triangular truncation of the atmosphere component occurs at wavenumber 159 (480 zonal grid and 240 meridional grids in post-processing). A hybrid coordinate system is used in the vertical direction with top to 10 hPa: a sigma system at the lowest model level gradually transforms into a pressure system in the lower stratosphere. The surface temperature is used as a boundary condition to determine the vertical profile within the five-layer soil model assuming vanishing heat fluxes at the bottom (10-m depth). The ocean component configuration is 320 (zonal) × 384 (meridional) grid points (meridionally about 0.3° in the near equatorial region) and 40 vertical levels. A solar absorption component based on specified monthly mean surface chlorophyll concentrations (Ohlmann 2003) is imbedded. The CICE v4.1 model details can be found in the study by Hunk and Lipscomb (2010). These model components are coupled by an OASIS3-MCT coupler interface (Larson et al. 2005). Atmosphere, ocean, and ice models exchange 36 variables including SST, surface fluxes, and ice components daily.

High quality climate forecasting relies on and requires improvement of climate models and use of advanced data assimilation methods that make full use of observation data. A synthesized atmosphere-ocean initialization scheme has been newly developed in this system, combining atmospheric 3-dimensional nudging and ocean 3-dimensional initialization using Ensemble Adjustment Kalman Filter methods (EAKF, Zhang et al. 2007; Anderson 2001). To generate perturbed initial conditions for the ensemble hindcasts and forecasts, three major steps are taken: 1) generation of model-compatible data set from analysis datasets; 2) nudging the model-compatible 3-D reanalysis data into the model; and 3) generation of perturbed ensemble initial conditions.

c. Hindcast simulation

Both systems have reproduced reforecast simulations for evaluating and calibrating the model simulation. APCC CCSM3 seasonal reforecasts have 10 ensemble members using the time-lagged method for a 1-month lead 6-month forecast. For a first-guess data of January 1, 1982, the atmosphere model is integrated for the period from 1971 to 1981 (11 years) using GODAS SST (Behringer et al. 1998). Using reproducing fluxes in an atmospheric simulation, the POP ocean model is executed for the same period. For the period 1982 to 2013, the initial condition for January 1, 1982 is nudged on day 1, 6, 11, 16, 21, and the last 5 days of every month using the GODAS vertical ocean temperature. Further details on the APCC CCSM3 reforecast are given in Jeong et al. (2008).

SCoPS has generated ensemble retrospective forecasts for the period 1982–2013 and real-time forecasts for the period 2014–current. Reforecast simulations commenced at fixed calendar dates — the 1st and 5th of each month — with 5 ensemble members perturbed following Gaussian distribution and integrated up to 7 months for a 1-month lead 6-month forecast. The ensemble initial conditions for January 1, 1982 are from the results from a 100-year free run SCoPS simulation. The initial data is assimilated every day from January 2, 1982 to December 31, 2013 using NCEP CFS reanalysis data (Saha et al. 2010) and World Ocean Database subsurface profile data including mechanical bathythermograph data (MBT), expendable bathythermograph data (XBT), profiling float data (PFL), ocean station data (OSD), conductivity-temperature-depth data (CTD), drifting buoy data (DRB), and Moored buoy data (MRB) (Boyer et al. 2013). In this system, the observed temperature (T) and salinity (S) are not only used to correct themselves but also to correct each other since the conservation of the T-S balance has been shown to be an important factor in successful data assimilation (Zhang et al. 2007). Vertically, only the profile data above 400 m is used since the deeper ocean is not expected to affect the seasonal forecast skill. Spatially, the observational data from the band between 50° S–50° N is used. Meanwhile, in real-time seasonal forecasting for the period 2014–current, the real-time combined ocean vertical profile dataset for temperature and salinity from the international Argo project is used for ocean initialization.

d. Evaluation

It is very well known that tropical large-scale circulations, such as Hadley, Walker, and monsoon are the most important driving source of general circulation at low latitudes, and their interannual variations largely impact climate characteristics in various regions. Tanaka et al. (2004) attempted to divide the divergent field in the upper troposphere into represented circulations such as Hadley, Walker, or global monsoon using the 200-hPa level seasonal velocity potential. They mentioned that the 200-hPa velocity potential very well represents overall characteristics such as intensity and variation in tropical circulations because they are each driven by different dynamical causes. Tanaka et al. (2004) defined the Hadley circulation as the axisymmetric part of the circulation, which represents the zonal mean field of the velocity potential. The monsoon circulation is defined as part of the seasonal variation of the deviation field. For this reason, the seasonal-mean is subtracted from the deviation field to define the monsoon circulation. More detailed definitions and analysis from field observations can be found in Tanaka et al. (2004). In this study, global monsoon circulation information using upper-level velocity potential from reanalysis and predicted results were evaluated following the methodology of Tanaka et al. (2004).

For other validations, SST data was obtained from the monthly National Oceanic and Atmospheric Administration (NOAA) Optimum Interpolation (OI) SST V2 (Reynolds et al. 2002). The air temperature at 2 m (T2m), mean sea level pressure (SLP), wind vector, and geopotential height data were obtained from the NCEP reanalysis 2 (RA2) and ERA-Interim reanalysis products (Kanamitsu et al. 2002; Dee et al. 2011) from 1982. The Global Precipitation Climatology Project (GPCP) version 2.1 combined precipitation dataset (Adler et al. 2003) and Asian Precipitation — Highly–Resolved Observational Data Integration Towards Evaluation of the Water Resources (APHRODITE) datasets (Yatagai et al. 2012) were used.

3. Results

a. Systematic biases

Figure 1 shows the spatial distribution of 1-month lead 3-month mean forecast biases of surface temperature, obtained from CCSM3 and SCoPS for the seasons of June-July-August (JJA) and December-January-February (DJF). CCSM3 and SCoPS represent the observed temperature patterns generally well in both seasons. However, the CCSM3 simulation shows slight warm or cold biases over the Eurasia region and significant warm biases over South America. In the SCoPS simulation, systematic biases in surface temperature prediction are significant, especially warm biases over North and South America and cold biases over the Eurasian region. Pattern correlation coefficients from both models are quite high, around 0.9 for both seasons. These biases pattern of 1-month lead-time forecast is almost same to those of 4-month lead-time forecast, although systematic biases get stronger as the lead time increases (not shown).

Figure 2 shows the spatial distribution of precipitation biases of model prediction in JJA and DJF. The GPCP observations show the peaks of the mean precipitation pattern over the intertropical convergence zone (ITCZ) on the Pacific as well as the western Pacific, South China Sea, and equatorial Indian Ocean (not shown here). The CCSM3 and SCoPS hindcast climatology generally well captures the observed wet regions, although there are different notable biases in the two models. In JJA, the predicted precipitation in CCSM3 tends to be overestimated over the equatorial central Pacific and parts of the Indian Ocean. Dry biases are also found in the Atlantic ITCZ, western Pacific, parts of the Indian Ocean, and the northeastern Pacific. Conversely, the SCoPS simulation generally tends to overestimate precipitation over the central Pacific ITCZ, the Atlantic ITCZ, and maritime continental regions. Some dry biases are also found in the central equatorial Pacific. In DJF, the CCSM3 hindcast shows wet biases over the eastern Pacific, northern central Pacific, and western Indian Ocean, and dry biases are exhibited over the eastern Indian Ocean. Conversely, the SCoPS simulation shows overestimated rainfall over the central Pacific ITCZ in the winter Northern Hemisphere. Pattern correlation coefficients from SCoPS are higher than those from CCSM3 throughout both seasons.

To examine seasonal prediction skill, the anomaly temporal correlation coefficient (TCC) of the sea surface temperature and precipitation between reanalysis data and 1-month lead hindcast anomalies are calculated for JJA and DJF (Figs. 3 and 4). The TCC for the sea surface temperature anomaly for each hindcast simulation compared to

NCEP RA2 data are shown in Fig. 3. Generally, the greatest prediction skill for sea surface temperature is in the tropics, especially in regions related to the ENSO, with the northern Pacific and equatorial Atlantic also showing high skill in both models. The SCoPS JJA prediction with 1-month lead shows higher prediction skill over the western Pacific, equatorial Pacific, and Indian Ocean than CCSM3. For DJF prediction, SCoPS shows higher skill in the northern Pacific and Indian Ocean than CCSM3. Although the TCC of temperature indicates the greatest skill over the tropical Pacific, it is quite low in most of the other areas. An impressive feature of SCoPS is that it maintains a higher TCC skill over the western northern Pacific and Indian Ocean than CCSM3 for both seasons.

Figure 4 shows the TCC of precipitation for JJA and DJF prediction with a 1-month lead. The prediction skill for precipitation is greater over the tropics than the extra-tropics and greater over ocean than land as known from other studies (Kim et al. 2012; Peng et al. 2011). These patterns from the seasonal prediction skill of CCSM3 and SCoPS are not much different from those of other seasonal prediction systems (e.g., Wang et al. 2009; Kim et al. 2012; Lee et al. 2014). In both season predictions, it is clear that the skill of SCoPS is higher than that of CCSM3 over the Indian Ocean and northern western Pacific, although some regions have lower skill.

Figure 5 shows the seasonal prediction skill as the averaged temporal correlation coefficient of the sea surface temperature, 2-m temperature, and precipitation anomalies. TCC is calculated for 1- to 4-month lead 3-month hindcasts (JJA, DJF) globally and for the East Asian region. The SST prediction skill is higher than the 2-m temperature and precipitation for JJA and DJF. The results indicate that the prediction skill generally decreases to the forecast lead time. Also, the prediction skill from SCoPS for all variables is significantly higher than CCSM3 for the 1-month lead for both seasons and both regions, although some variables show lower skill for a long lead time. In particular, the SST prediction skill from SCoPS is about 0.5 for the East Asian region.

Climate variability as well as climatology is also important factor to assess the seasonal prediction skill. Many studies have analyzed the signal to noise (SN) ratio to assess the predictability of seasonal prediction system with lead-time (Peng et al. 2011; Peng et al. 2014). Due to the APCC seasonal forecast system is for 3-month or longer target season, SN ratio for a fixed target season of JJA from CCSM3 and SCoPS with 1 and 4 month lead-time are shown in figures 6 and 7. Here, 'signal' indicates standard deviations of the ensemble mean, and 'noise' indicates standard deviations of ensemble members about ensemble mean. In other words, the SN ratio is computed as the ratio of variance of ensemble means, and variance of individual forecasts from the ensemble mean forecast. Larger (small) SN ratio indicates higher (lower) predictability.

Shown in Fig. 6 is the SN ratio for SST, precipitation, and 200 hPa geopotential heights from CCSM3 and SCoPS with 1 month lead-time. For SST, SN ratio from both systems shows highest in the eastern equatorial tropical Pacific related to the ENSO. CCSM3 show high SN ratio in high latitude region in southern hemisphere, while SCoPS show that in northern Pacific, Greanland, as well as Atlantics. For SN ratio for precipitation prediction with 1-month lead forecast is largest in the tropics and decreases in the extratropical latitudes for both systems. For 200 hPa geopotential height, the high SN ratio is also concentration in Tropics for both models, but SCoPS show higher SN ratio in broaden region than CCSM3. Also, the reason of low SN ratio in extrtropics is large standard deviation of individual forecasts from the ensemble mean forecast (i.e., noise) (not shown). This finding about 'noise' in extratropics is consistent with Peng et al. (2011).

SN ratio for atmospheric variables from CCSM3 and SCoPS with 4 month lead-time is shown in figure 7. Compared to the results with 1 month lead-time in Fig. 6, SN ratio for all variables shows decrease to the lead-time. For structure of SN ratio for SST, precipitation from CCSM3 and SCoPS are not much differ each other. However, for SN ratio of 200 hPa geopotential height, SCoPS is still higher than CCSM3 in tropics. These results indicate that large-scale circulation related to the height from SCoPS is more reliable than that from CCSM3 with long lead-time, although both systems have quite big uncertainty in precipitation. Also, SST forecasts from both systems quite well stay high signal with 4-month lead-time, it is due to the SST characteristic with slowing vary.

It is well known that the ENSO is the main driver of interannual variability in the tropics. A good representation of it and its teleconnections are very important for good climate prediction skill. Figure 8 shows the results of a comparison between the lead time dependence of the SST TCC and RMSE in the Niño 3.4 and Niño 3 regions, with the OISST observational dataset for hindcasts initialized in May and November. Overall, the skill of the Niño indices is generally good, although the skill tends to decrease with lead time. Both SCoPS and CCSM3 exhibit higher skill for the November-initialized hindcast than the May-initialized hindcast. SCoPS shows slightly higher skill than CCSM3 until the 5-month lead time over the Niño 3.4 and Niño 3 regions for the hindcast initialized in November. However, the skill of SCoPS May-initialized hindcast is not much more different than CCSM3 for both indices. However, the RMSE of the SST from SCoPS for the Niño 3.4 region in the run initialized in May is worse than that from CCSM3 (Fig. 8c), due to the fact that there are cold biases in the tropical Pacific in the SCoPS prediction.

b. East Asian summer climate variability

First, the velocity potential and divergent wind at 200 hPa averaged for JJA are plotted to examine the summer monsoon variability (Figs. 9a, b, c). In the observed velocity potential distributions (Fig. 9a), a positive peak with a value of nearly 20 ($\times 10^6$ m^2 s^{-1}) is located northwest of the Philippines in JJA. The minimum is seen over the southern Atlantic Ocean, with a value of -10 ($\times 10^6$ m^2 s^{-1}). Hereafter, the velocity potential "units" of measurement are assumed to be 10^6 m^2 s^{-1} for simplicity. A strong divergent wind related to the Hadley circulation is shown from the northern to southern Hemisphere. The combined Hadley, Walker, and monsoon circulation shows a strong convection located in the Philippines. Both 1-month lead hindcast simulations generally represent the 200-hPa velocity potential pattern well, and the positive and negative peaks are also captured. However, the SCoPS simulation tends to overestimate its intensity, while the CCSM3 run shows a weak intensity over the peak regions in summer (Figs. 9b, c).

To extract the monsoon variability, following Tanaka et al. (2004) deviation from the zonal and annual mean of velocity potential is calculated (Figs. 9d, e, f). In JJA, the observations show a dominant positive (negative) peak located over East Asia (Pacific and Atlantic oceans). This is a feature of the Northern Hemisphere summer, which includes an upper air divergence over East Asia and an upper air convergence over the Pacific and Atlantic oceans related to the East Asian summer monsoon. A convection center located near the Philippines in the mean velocity potential field (Fig. 9a) can be explained by a superposition between one over land associated with the monsoon circulation (Fig. 9d) and another near the equator associated with the Walker circulation (not shown). CCSM3 underestimates the upper air divergence over East Asia and splits the peak into two over the eastern Pacific, while SCoPS results are closer to the observations than those from the CCSM3 hindcast (Fig. 9f). Based on the results, we conclude that the overestimated mean velocity potential in the SCoPS simulation (Fig. 9c) is due to the enhanced Hadley circulation (not shown), and the underestimated mean velocity potential in CCSM3 (Fig. 9b) is due to the weak simulated monsoon circulation (Fig. 9e). Also, it is sure that large-scale circulation features from SCoPS can expect to more realistic variability related to the monsoon than that from CCSM3.

Figure 10 shows the climatological mean precipitation and the 850-hPa zonal wind over the East Asian region during summer (June–August) in observations (GPCP and APHRODITE for precipitation; ERA-Interim reanalysis for zonal wind) and hindcasts from CCSM3 and SCoPS. Note that horizontal resolution of GPCP is 2.5° × 2.5°, while that of APHRODITE is 0.25° × 0.25° with land-only data. In the climatology for JJA, two major areas of strong precipitation are observed. One is the main precipitation band related to the ITCZ over the tropics, and the other one is the extending rainband from southern China to Japan, which is related to the East Asian summer monsoon (EASM) (Figs. 10a, b). Local monsoon precipitation maxima are in the oceanic convergence regions over the northeastern Arabian Sea and the Bay of Bengal, and west of the Philippines.

CCSM3 reproduces the features well; however, precipitation over the northwestern Pacific is underestimated, and precipitation over the Indian Ocean and western equatorial Pacific tends to be overestimated (Fig. 10c). Related to this, the low-level monsoon flow pattern is shifted to the precipitation region. The precipitation from

SCoPS shows a slight overestimation. Narrow and strong bands of precipitation are indicated over the western areas of India, Indochina, and the Philippines in the high-resolution APHRODITE data. This extremely localized pattern is known to be due to convection generated by narrow mountain areas (Xie et al. 2006; Lee et al. 2013; Ham et al. 2016). The observed pattern is very well represented in the SCoPS hindcast, due to its higher horizontal resolution as compared to CCSM3. Moreover, the SCoPS simulation represents the area over China, Korea, and Japan remarkably well, where the seasonal prediction captures the zonally elongated rainband associated with the Changma front (Fig. 10d).

Figure 11 shows latitude-time cross sections for the summer precipitation cycle and 850-hPa zonal winds on two longitudes (70–80 °E and 120–130 °E), which are related to the Indian and East Asian monsoon. Because precipitation from CCSM3 and SCoPS is usually focused on the 1-month lead 3-month prediction skill in operational seasonal forecasts, four hindcast datasets from runs initialized in February, May, August, and November were merged to validate the represented annual cycle of precipitation and winds. Both hindcasts generally represent the seasonal propagation of precipitation in the Indian (70–80 °E) and East Asian monsoon regions (120–130 °E), compared to the GPCP and reanalysis data. For example, the northward rainband related to the Indian monsoon (April to July) is generally well represented. However, the CCSM3 simulation exhibits a weaker peak in the northward propagated rainband as well as strong precipitation over the subtropics and tropics, compared to observations. In the SCoPS simulation, the peak of the northward precipitation band and the low-level wind are captured, although slightly overestimated. However, note that the GPCP observation does not represent orographic heavy rainfall well due to its low resolution. For the East

Asian monsoon region, a split rainband is shown during June to August, with one arm over South China Sea, related to the ITCZ, and another over the subtropics, which is related to the Changma front. Both models exhibit the rain peak over the ITCZ well; however, CCSM3 shows exaggerated precipitation over the equatorial rainband, even in winter. In the SCoPS annual cycle, the two peak rain seasons are represented quite well, but slightly overestimated. Remarkably, the northward migrated rainband related to the Changma during May to August is also captured by SCoPS.

In Fig. 12, the capability of CCSM3 and SCoPS in simulating the spatial pattern and interannual variability of the Asian summer monsoon is examined using the monsoon index developed by Lee et al. (2014). The EASM index is defined as the zonal wind anomaly at 850 hPa, averaged over the region between 5–10° N and 130–150° E minus the average over 25–30° N and 110–130° E. The JJA-mean monsoon indices from the ensemble reforecasts initialized in May were used. The correlation coefficient of the EASM index between the reanalysis and the SCoPS prediction (0.743) is higher than the CCSM3 prediction (0.519). Based on the results, SCoPS shows a credible representation of monsoon circulation for this region, with useful levels of skill for the East Asian summer monsoon prediction.

c. East Asian winter climate variability

The East Asian winter monsoon (EAWM) is the dominant climate feature over East Asia during the boreal winter. It leads to significant impacts on the weather and climate over the East Asian regions (Chen et al. 2005; Zhou et al. 2007; Li and Yang 2010; Jiang et al. 2013). The EAWM consists of subsystems such as the Siberian high, Aleutian low, East Asian trough, low-level northerly wind, and high-level East Asian jet stream. It is well known that a strong EAWM is characterized by a strong Siberian high, intensified East Asian jet stream, a deepened East Asian trough, strong northerly wind over East Asia, and frequent cold surges (Ding and Sikka 2006; Park et al. 2011; Jiang et al. 2013). Many climate forecast models show reasonable skill in the East Asian summer monsoon prediction. However, the EAWM prediction skill on climate forecast systems is still not fully known, although a few studies have examined the predictability of the EAWM in various climate prediction models (Kim et al. 2012; Jiang et al. 2013). In this study, the climatological characteristics and interannual variation of the EAWM were compared with observations and reanalysis data to confirm the seasonal prediction skills. Also, the prediction skill for the Arctic Oscillation (AO), which is known to be a dominant feature of winter climate variability in East Asia, was evaluated for the CCSM3 and SCoPS hindcasts initialized in November.

The northern hemisphere winter (DJF) variation in velocity potential for the climatological mean with 200-hPa divergent winds is shown in Fig. 13. In the observed distributions, the positive peak shows its full weakness as a value of 12 units and it is located to the equatorial western Pacific (Fig. 13a). The location of the negative peak is near western Africa. The center related to the Australian monsoon is located to the north of Australia. Both hindcast simulations represent the positive and negative peaks of velocity potential at 200 hPa well (Figs. 13b, c). The SCoPS simulation plots resemble observations more than the CCSM3 simulation because the divergent wind from CCSM3 is stronger than that from SCoPS. Also, the pattern correlation of upper-level velocity potential fields from SCoPS (0.85) is higher than that from CCSM3 (0.57).

Following Tanaka et al. (2004), the deviation from the zonal and annual mean of the velocity potential is calculated for the northern hemisphere winter monsoon circulation (Figs. 13d, e, f). In the observations, there are negative peaks over East Asia and positive peaks over the Pacific. A reversal in the pattern between summer and winter explains the monsoon circulation quite well (See also Figs. 9). The SCoPS simulation captures the observed peaks related to the East Asian winter monsoon feature, while the CCSM simulation shows a divided peak over the Australia region. Also, the SCoPS simulation is closer to the observations in terms of intensity than the CCSM3 hindcast. The pattern correlation of monsoon circulation fields from SCoPS (0.88) is also significantly higher than that from CCSM3 (0.28).

In the lower troposphere, the characteristics of the EAWM are the contrast between the Siberian high and the Aleutian low. These systems lead to strong northwesterlies over the eastern marginal regions of the Siberian high (Fig. 14a). This monsoon system is also related to the East Asian trough along the Korea and Japan regions in the middle troposphere and the maximization of the jet stream over southeastern Japan in the upper troposphere (Fig. 14d). The CCSM3 and SCoPS hindcasts represent the climatological features related to the EAWM well (Figs. 14b, c, e, f). However, the CCSM3 hindcast shows a stronger Siberian high and Aleutian low, stronger cyclonic circulation in the trough region, and stronger jet stream than observations. The SCoPS hindcast shows some biases, including a weak Siberian high and Aleutian low; however, the maximum jet stream in the upper troposphere and the trough in the middle troposphere are better captured than in CCSM3. In addition, the hindcasts have biases in simulating the divergent maritime continental winds compared to observations, with easterlies from CCSM3 and westerlies from SCoPS. The 500-hPa geopotential height in the CCSM3 simulation is higher than observed except for northeastern China, resulting in a weaker than observed East Asian trough. On the other hand, the SCoPS hindcast shows a lower geopotential height than observed except along Korea and Japan, resulting in a weaker than observed trough. SCoPS generally predicts a weaker zonal wind along the westerly jet stream than observed.

To confirm the prediction skill of the models for interannual variation, the dynamical EAWM index is shown in Fig. 15. This index was proposed by Li and Yang (2010) to measure the interannual variability of the EAWM and is defined as the domain-averaged 200-hPa zonal wind shear. Compared to previous indices, this EAWM index accounts for several factors influencing the monsoon (e.g., the Arctic Oscillation and ENSO) and better elucidates the physical processes associated with the EAWM (Li and Yang 2010; Wang and Chen 2010; Wang et al. 2010). SCoPS realistically represent the observed variation in most years, with a correlation coefficient of 0.459. However, CCSM3 shows poorer prediction skill than SCoPS, with a correlation coefficient of 0.245.

The Arctic Oscillation (AO) is important climate variability with EAWM in East Asia, especially during boreal winter. Its intensity and variability play a significant role to surface temperature, precipitation, and large-scale circulation for extratropical region in northern hemisphere. However, the prediction skill of the AO variation on a seasonal timescale is still poor in dynamical forecast systems (Johansson 2007; Kim et al. 2012; MacLachlan et al. 2015). In this study, the represented AO in CCSM3 and SCoPS were compared with the NCEP reanalysis data. Following the definition of AO by Thompson and Wallace (1998), the AO index was calculated as the principal component (PC) of the first empirical orthogonal function (EOF) mode for monthly mean SLP anomalies during boreal winter (DJF).

Figure 16 shows the results of comparison of the PC time series from RA2, CCSM3, and SCoPS, for hindcast simulations with November initialization. Results from the all ensemble prediction are indicated in red (SCoPS) and blue (CCSM3) shading areas. To compare the prediction skill, the ensemble-averaged AO indices from both models and reanalysis were plotted by solid lines. Both PC time series capture the interannual variation shown in reanalysis data. The anomaly correlation coefficient between the observed and predicted AO index is 0.58 for SCoPS but only 0.23 for CCSM3. Especially, the SCoPS simulation captured the variation in strong positive/negative phase of AO for the recent period of 2009–2012.

Figure 17 shows the SLP patterns regressed onto the leading PC from reanalysis data and both hindcasts. It was used for individual EOF analysis from each model ensemble member and a composite map of those regression patterns was plotted. The pattern from RA2 has a dipole structure over the Arctic, northeastern Pacific, and Atlantic Ocean (Fig. 17a). CCSM3 represents the negative regression pattern over Arctic well. However, the positive patterns over Pacific and Atlantic Ocean were totally not captured. Although SCoPS shows a significant weak AO negative pattern over the Arctic and the center of the positive regression anomaly over the Atlantic Ocean is parted, the positive center remains over the northeastern Pacific as in the observation. The reasonable prediction skill of the AO in SCoPS gives an expectation of good reliability for extratropical winter surface temperature predictions over East Asia.

4. Summary and conclusion

In this paper, a new APCC in-house model, namely SCoPS, is introduced. SCoPS is a state-of-the-art seasonal prediction system based on a fully-coupled climate model, coupling atmosphere, ocean, and sea ice with integrated atmosphere-ocean initialization processes. The SCoPS initialized data for 10-member ensembles are assimilated by NCEP CFS data and several subsurface profile data. The ensemble hindcast runs are conducted with SCoPS for 32-year runs (1982−2013).

This study evaluated the systematic biases of hindcast climatology, large-scale features, and the basic performance of seasonal forecasting for major climate variability from CCSM3 and SCoPS. A special focus was placed on the fidelity of the systems to reproduce and forecast phenomena that are closely related to the East Asian monsoon system. In particular, to validate the large-scale circulation related to the East Asian monsoon system, the global divergent field in the upper troposphere was used following Tanaka et al. (2004).

Overall both CCSM3 and SCoPS exhibit realistic representations of the basic climate state, although systematic biases were found for sea surface temperature, 2-m temperature, and precipitation. To examine the seasonal prediction skill, the temporal correlation coefficients of sea surface temperature and precipitation between observation and the anomalies of each model were also validated for summer and winter. Generally, the sea surface temperature has its greatest prediction skill in the tropics, especially in the ENSO region. Both models also exhibit high skill over the northern Pacific and equatorial Atlantic. SCoPS shows high prediction skill over almost all regions compared to CCSM3. The averaged temporal anomaly correlation coefficient for sea surface temperature, 2-m temperature, and precipitation from SCoPS is also higher than those from CCSM3. However, the RMSE for SST from SCoPS with 1-month lead for DJF in the Niño 3 and Niño 3.4 regions is worse than that from CCSM3. This is because there are cold biases over the tropical Pacific in SCoPS.

Notably, SCoPS captures the northward migrated rainband related to the East Asian summer monsoon system. Further, SCoPS shows a higher correlation coefficient between the observed and predicted monsoon indices than CCSM3 for both summer and winter seasons. The SCoPS simulation shows useful skill in predicting the Arctic Oscillation. Consequently, SCoPS is more skillful than CCSM3 in predicting the seasonal climate variability, including the ENSO, East Asian summer and winter monsoon, and the Arctic Oscillation.

Based on these results, the SCoPS seasonal forecast results are provided to the APCC multi-model ensemble (MME) system as a new APCC operational model, which is changed from CCSM3 since November 2017. Validation of real-time forecast skill is an ongoing work-in-progress. Other climate variabilities including ENSO, Indian Niño, Atlantic Niño, Pacific-North America pattern will be evaluated. Moreover, an operational subseasonal forecast system is on the drawing board.

Acknowledgments

This research was supported by the APEC Climate Center. Also, this study was supported by the Korea Meteorological Administration. We especially thank KMA's supercomputer management division for providing us with the supercomputer resource and consulting on technical support. Also, this research is based on APCC Project (2015), “Development of APCC Seamless Prediction System” by APCC with a research group of the University of Hawaii, USA. Dr. Bin Wang acting as PI of the project leads and directs the APCC project (2012-2015), ‘Development of APCC Seamless Prediction System’. Dr. Baoqiang Xiang develops the atmosphere-ocean-sea ice coupled model system. Dr. Shu Wu develops the EAKF initialization and observational data pre-process package. Dr. Joshua Xiouhua Fu develops the 3D-nudging atmosphere

initialization. Some of ocean data were collected and made freely available by the International Argo Program and the national programs that contribute to it. (http://www.argo.ucsd.edu, http://argo.jcommops.org). The Argo Program is part of the Global Ocean Observing System.

References

Adler, R. F., and Coauthors, 2003: The Version 2 Global Precipitation Clilmatology Project (GPCP) monthly precipitation analysis (1979-Present). J. Hydrometeo., 4, 1147-1167.

APCC Project Report, 2015: Development of APCC Seamless Prediction System. *Final Report (internal report)*, 103pp, APEC Climate Center.

Anderson, D., and coauthors, 2007: Development of the ECMWF seasonal forecast System 3. *ECMWF Technical Memorandum 503*.

Anderson, J. L., 2001: An ensemble adjustment Kalman filter for data assimilation. *Mon. Wea. Rev.*, **129**, 2884-2903.

Arribas, A., and Coauthors, 2011: The GloSea4 ensemble prediction system for seasonal forecasting. *Mon. Wea. Rev.*, **139**, 1891-1910.

Bechtold, P., M. Köhler, T. Jung, F. Doblas-Reyes, M. Leutbecher, M. J. Rodwell, F. Vitart, and G. Balsamo, 2008: Advances in simulating atmospheric variability with the ECMWF model: From synoptic to decadal time-scales. *Quart. J. Roy. Meteor. Soc.*, **134**, 1337-1351. doi:10.1002/qj.289.

Behringer, D., M. Ji, and A. Leetmaa, 1998: An improved coupled model for ENSO prediction and implications for ocean initialization. Part I: The ocean data assimilation system, *Mon. Wea. Rev.*, **126**, 1013-1021.

Boyer, T.P., and Coauthors, 2013: World Ocean Database 2013, NOAA Atlas NESDIS 72, S. Levitus, Ed., A. Mishonov, Technical Ed.; Silver Spring, MD, 209 pp., http://doi.org/10.7289/V5NZ85MT

Briegleb, B. P., C. M. Bitz, E. C. Hunke, W. H. Lipscomb, M. M. Holland, J. L. Schramm, and R. E. Moritz, 2004: Scientific description of the sea ice component in the Community Climate System Model, Version Three. *Tech. Rep. NCAR/TN-463+STR*, National Center for Atmospheric Research, Boulder, CO, 78 pp.

Chen, W., S. Yang, and R. Huang, 2005: Relationship between stationary planetary wave activity and the East Asian winter monsoon, *J. Geophys. Res.*, **110**, doi:10.1029/2004JD005669.

Cohen, J., and J. Jones, 2011: A new index for more accurate winter predictions. *Geophys. Res. Lett.*, **38**, L21701, doi:10.1029/2011GL049626.

Collins, W. D., and Coauthors, 2004: Description of the NCAR Community Atmosphere Model (CAM3). *Tech. Rep. NCAR/TN-464+STR*, National Center for Atmospheric Research, Boulder, CO, 226pp.

-----------, and Coauthors, 2006: The formulation and atmospheric simulation of the Community Atmosphere Model version 3 (CAM3). *J. Climate*, **19**, 2144-2161.

Dee, D. P., and Coauthors, 2011: The ERA-Interim reanalysis: configuration and performance of the data assimilation system. *Quart. J. Roy. Meteor. Soc.*, **137**, 553-597.

Derome, J., H. Lin, and G. Brunet, 2005: Seasonal forecasting with a simple general circulation model: Predictive skill in the AO and PNA. *J. Clilmate*, **18**, 597-609, doi:10.1175/JCLI-3289.1.

Dickinson, R. E., K. W. Oleson, G. Bonan, F. Hoffman, P. Thormton, M. Vertenstein, Z.-L. Yang, and X. Zeng, 2006: The Community Land Model and its climate statistics as a component of the Community Climate System Model. *J. Climate*, **19**, 2302-2324.

Ding, Y., and D. R. Sikka, 2006: Synoptic systems and wather, in The Asian Monsoon, edited by B. Wang, pp. 141-201, Praxis, New York.

Dirkson, A., W. J. Merryfield, A. Monahan, 2017: Impacts of Sea ice thickness initialization on seasonal arctic sea ice predictions. *J. Climate*, **30,** 1001-1016.

Folland, C.K., A. A. Scaife, J. Lindesay, D. B. Stephenson, 2012: How potentially predictable is northern European winter climate a season ahead? *Int. J. Climatol.*, **32**, 801-818, doi:10.1002/joc.2314.

Hagemann, S., K. Arpe, and E. Roeckner, 2006: Evaluation of the hydrological cycle in the ECHAM5 model. *J. Climate*, **19**, 3810-3827.

Ham, S., S.-Y. Hong, and S. Park, 2014: A study on air-sea interaction on the simulated seasonal climate in an ocean-atmosphere coupled model. *Clim. Dyn.*, **42**, 1175-1187.

Ham, S., J.-W. Lee, K. Yoshimura, 2016: Assessing future climate changes in the East Asian summer and winter monsoon using regional spectral model. *J. Meteor. Soc. Japan*, **94A**, 69-87.

Ham, Y.-G., and M. M. Rienecker, 2012: Flow-dependent empirical singular vector with an ensemble Kalman filter data assimilation for El Niño prediction. *Clim. Dyn.*, **39**, 1727-1738.

Hunk, E. C., and W. H. Lipscomb, 2010: CICE: The Los Alamos Sea Ice Model Documentation and Software User's Manual Version 4.1. LA-CC-06-012, T-3 Fluid Dynamics Group, Los Alamos National Laboratory, Los Alamos N.M.

Hwang, Y.-T., and D. M. W. Frierson, 2013: Link between the double-intertropical convergence zone problem and cloud biases over the Southern Ocean. Proc. Natl. Acad. Sci., 110, 4935-4940.

Jeong, H.-I., and Coauthors, 2008: Experimental 6-month hindcast and forecast simulation using CCSM3. *APCC 2008 Technical Report*, APEC Climate Center.

Jiang, X., S. Yang, Y. Li, A. Kumar, W. Wang, and Z. Gao, 2013: Dynamical prediction of the East Asian winter monsoon by the NCEP Climate Forecast System. *J. Geophys. Res. Atmos.*, **118**, 1312-1328, doi:10.1002/jgrd.50193.

Johansson, Å., 2007: Prediction skill of the NAO and PNA from daily to seasonal time scale. *J. Climate*, **20**, 1957-1975, doi:10.1175/JCLI4072.1.

Kanamitsu, M. and Coauthors, 2002: NCEP dynamical seasonal forecast system 2000. *Bull. Am. Meteor. Soc.*, **83**, 1019-1037.

Kim, H.-M., P. J. Webster and J. A. Curry, 2012: Seasonal prediction skill of ECMWF System 4 and NCEP CFSv2 retrospective forecast for the Northern Hemisphere Winter. *Clim. Dyn.*, **39**, 2957-2973.

Kim, S. T., H.-I. Jeong, and F.-F. Jin, 2017: Mean bias in seasonal forecast model and ENSO prediction error. *Sci. Rep.*, **7,** doi: 10.1038/s41598-017-05221-3.

Koster, R. D., and Coauthors, 2010: Contribution of land surface initialization to subseasonal forecast skill: First results from a multi-model experiment. *Geophys. Res. Lett.*, **37,** L02402, doi:10.1029/2009GL-041677.

Kug, J.-S., Y.-G. Ham, M. Kimoto, F.-F. Jin, and I.-S. Kang, 2010: New approach for optimal perturbation method in ensemble climate prediction with empirical singular vector. *Clim. Dyn.*, **35**, 331-340, doi:10.1007/s00382-009-0664-y.

Kusunoki, S., M. Sugi, A. Kitoh, C. Kobayashi, K. Takano, 2001: Atmospheric seasonal predictability experiments by the JMA AGCM. *J. Meteor. Soc. Japan*, **79**, 1183-1206.

Larson, J., R. Jacob, and E. Ong, 2005: The Model Coupling Toolkit: A new fortran90 toolkit for building Multiphysics parallel coupled models. *Int. J. High Perf. Comp. App.*, **19**, 277-292.

Lee, J.-W., S.-Y. Hong, E.-C. Chang, M.-S. Suh, and H.-S. Kang, 2013: Assessment of future climate change over East Asia due to the RCP scenarios downscaled by GRIMs-RMP. *Clim. Dyn.*, **42**, 733-747.

Lee, M.-I., H. S. Kang, D. Dim, D. Kim, H. Kim, and D. Kang, 2014: Validation of the experimental hindcasts produced by the GloSea4 seasonal prediction system. *Asia-Pac. J. Atmos. Sci.*, **50(3),** 307-326.

Li, Y., and S. Yang, 2010: A dynamical index for the East Asian winter monsoon, *J. Climate*, **23**, 4255-4262.

Lin, S. and R. B. Rood, 1996: Multidimensional flux-form semi-Lagrangian transportation schemes. *Mon. Wea. Rev.*, **124**, 2046-2070.

MacLachlan, C., and Coauthors, 2015: Global Seasonal forecast system version 5 (GloSea5): a high-resolution seasonal forecast system. *Quart. J. Roy. Meteor. Soc.*, **141**, 1072-1084. doi:10.1002/qj.2396.

Min, Y.-M., V. N. Kryjov, and S. M. Oh, 2014: Assessment of APCC multimodel ensemble prediction in seasonal climate forecasting: Retrospective (1983–2003) and real-time forecasts (2008–2013), *J. Geophys. Res. Atmos.*, **119,** 12,132–12,150, doi:10.1002/2014JD022230.

Molteni, F., R. Buizza, T. N. Palmer, and T. Petroliagis, 1996: The ECMWF ensemble prediction system: Methodology and validation. *Quart. J. Roy. Meteor. Soc.*, **122**, 73-119. doi: 10.1002/qj.49712252905.

Molteni, F., and coauthors, 2011: The new ECMWF seasonal forecast system (System 4). ECMWF Technical Memorandum No. 656.

Ohlmann, J. C., 2003: Ocean radiant heating in climate models. *J. Climate*, **16**, 1337-1351.

Oleson, K. W., and Coauthors, 2004: Technical description of the Community Land Model (CLM). *Tech. Rep. NCAR/TN-461+STR*, National Center for Atmospheric Research, Boulder, CO, 174pp.

Park, T.-W., C.-H. Ho, S. Yang, 2011: Relationship between the Arctic Oscillation and cold surges over East Asia. *J. Climate*, **24**, 68-83.

Peng, P., A. Kumar, W. Wang, 2011: An analysis of seasonal predictability in coupled model forecasts. *Clim. Dyn.*, **36**, 419-430.

Peng, P., A. Kuma, B. Jha, 2014: Climate mean, variability and dominant patterns of the Northern Hemisphere winter mean atmospheric circulation in the NCEP CFSv2. *Clim. Dyn.*, **42,** 2783-2799.

Prodhomme, C., F. Doblas-Reyes, O. Bellprat, E. Dutra, 2016: Impact of land-surface initialization on sub-seasonal to seasonal forecasts over Europe. *Clim. Dyn.*, **47,** 919-935.

Reynolds, R. W., N.A. Rayner, T.M. Smith, D.C. Stokes, and W. Wang, 2002: An improved in situ and satellite SST analysis for climate. J. Climate, 15, 1609-1625. [NOAA_OI_SST_V2 data provided by the NOAA/OAR/ESRL PSD, Boulder, Colorado, USA, from their Web site at http://www.esrl.noaa.gov/psd/]

Roeckner, E., G. Buml, L. Bonaventura, and Coauthors, 2003: The atmospheric general circulation model ECHAM5. Part I: Model description. MPI Reprot 349, Max Planck Institute for Meteorology, Hamburg, Germany, 127pp.

Saha, S., and Coauthors, 2006: The NCEP climate forecast system. *J. Climate*, **19**, 3483-3517.

-------------, and Coauthors, 2010: The NCEP climate forecast system reanalysis. *Bulletin of the American Meteorological Society*, **91,** 1015-1057, doi:10.1175/2010BAMS3001.1

--------------, and Coauthors, 2014: The NCEP climate forecast system version 2. *J. Climate*, **27**, 2185-2208.

Smith, R. D., and P. R. Gent, 2002: Reference manual for the Parallel Ocean Program (POP), ocean component of the Community Climate System Model (CCSM2.0 and 3.0). Tech. Rep. LA-UR-02-2484, Los Alamos National Laboratory. [Available online at http://www.ccsm.ucar.edu/models/ccsm3.0/pop.]

Tanaka, H. L., N. Ishizaki and A. Kitoh, 2004: Trend and interannual variability of Walker, monsoon and Hadley circulations defined by velocity potential in the upper troposphere, *Tellus*, **56A**, 250-269.

Thompson, D. W. J., and J. M. Wallace, 1998: The Arctic Oscillation signature in the wintertime geopotential height and temperature fields. *Geophys. Res. Lett.*, **25**, 1297-1300, doi:10.1029/98GL00950.

Wang, B., and Coauthors, 2009: Advance and prospectus of seasonal prediction: assessment of the APCC/CliPAS 14-model ensemble retrospective seasonal prediction (1980-2004). *Clim. Dyn.*, **33**, 93-117, doi:10.1007/s00382-008-0460-0.

Wang, L., and W. Chen, 2010: How well do existing indices measure the strength of the East Asian winter monsoon? *Adv. Atmos. Sci.*, **27**, 855-870.

-----------, W. Chen, W. Zhou and Coauthors, 2010: Effect of the climate shift around mid 1970s on the relationship between wintertime Ural blocking circulation and East Asian climate, *Int. J. Climatol.*, **30**, 153-158.

Xiang, B., B. Wang, Q. Ding, F.-F. Jin, and Coauthors, 2012: Reduction of the thermocline feedback associated with mean SST bias in ENSO simulation. *Clim. Dyn.*, **39**, 1413-1430.

Xie, S.-P., H. Xu, N.H. Saji, Y. Wang, and W. T. Liu, 2006: Role of narrow mountains in large-scale organization of Asian monsoon convection. *J. Climate*, **19**, 3420-3429.

Yatagai, A., K. Kamiguchi, O. Arakawa, A. Hamada, N. Yasutomi, and A. Kitoh, 2012: APHRODITE: Constructing a long-term daily gridded precipitation dataset for Asia based on a dense network of rain gauges. *Bull. Amer. Meteor. Soc.*, **93**, 1401-1415.

Zhang, G. J., and H. Wang, 2006: Toward mitigating the double ITCZ problem in NCAR CCSM3. *Geophys. Res. Lett.*, **33,** L06709, doi:10.1029/2005GL025229.

Zhang, S., M. J. Harrison, A. Rosati, and A. Wittenberg, 2007: System design and evaluation of coupled ensemble data assimilation for global oceanic climate studies. *Mon. Wea. Rev.*, **135**, 3541-3564.

Zhou, W., C. Li, and X. Wang, 2007: Possible connection between Pacific Oceanic interdecadal pathway and East Asian winter monsoon, *Geophys. Res. Lett.*, **34**, L01701.

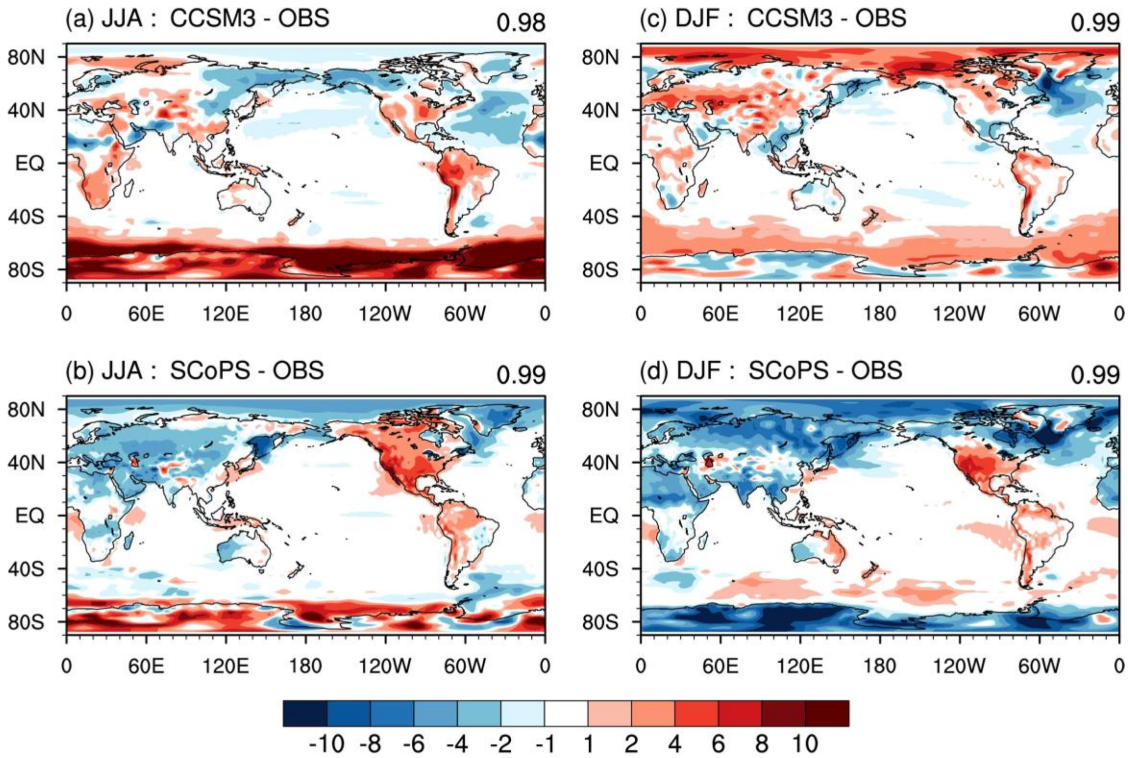

Fig. 1. Spatial distribution of climatological summer (left) and winter (right) of the surface temperature biases (model minus observation) for (a), (c) CCSM3 and (b), (d) SCoPS. Top-right value indicates the pattern correlation coefficient between observation and each prediction.

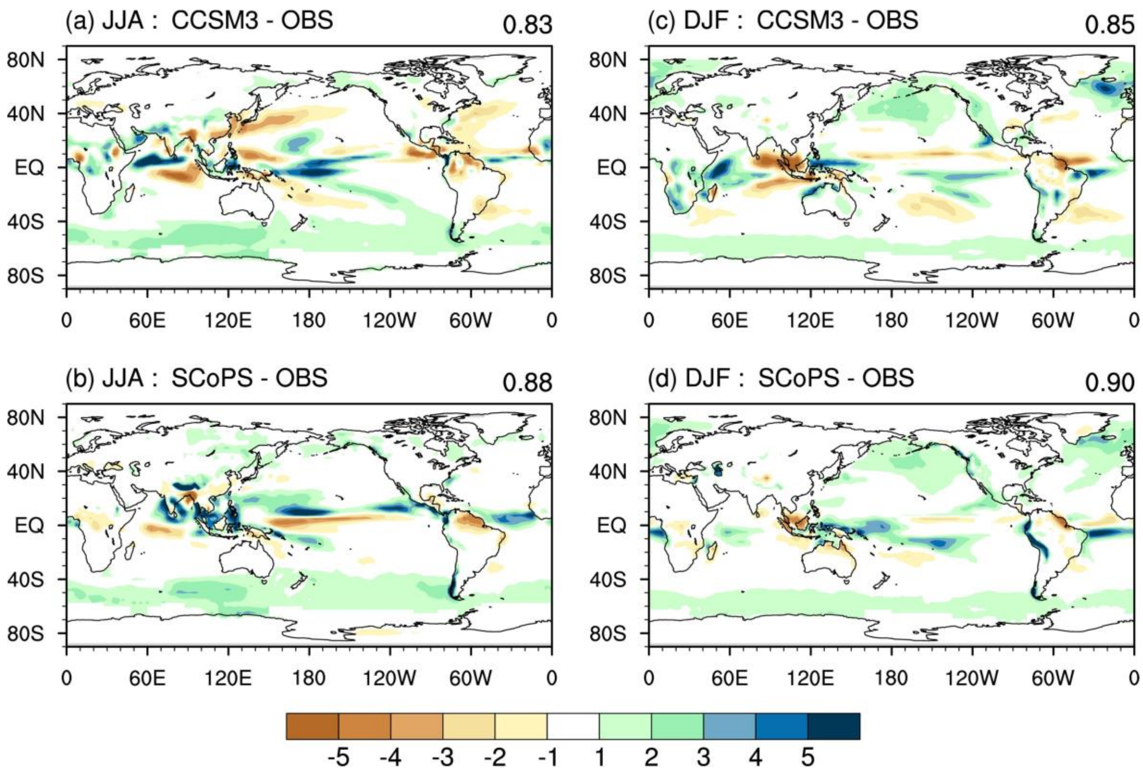

Fig. 2. Same as Fig. 1, but for precipitation.

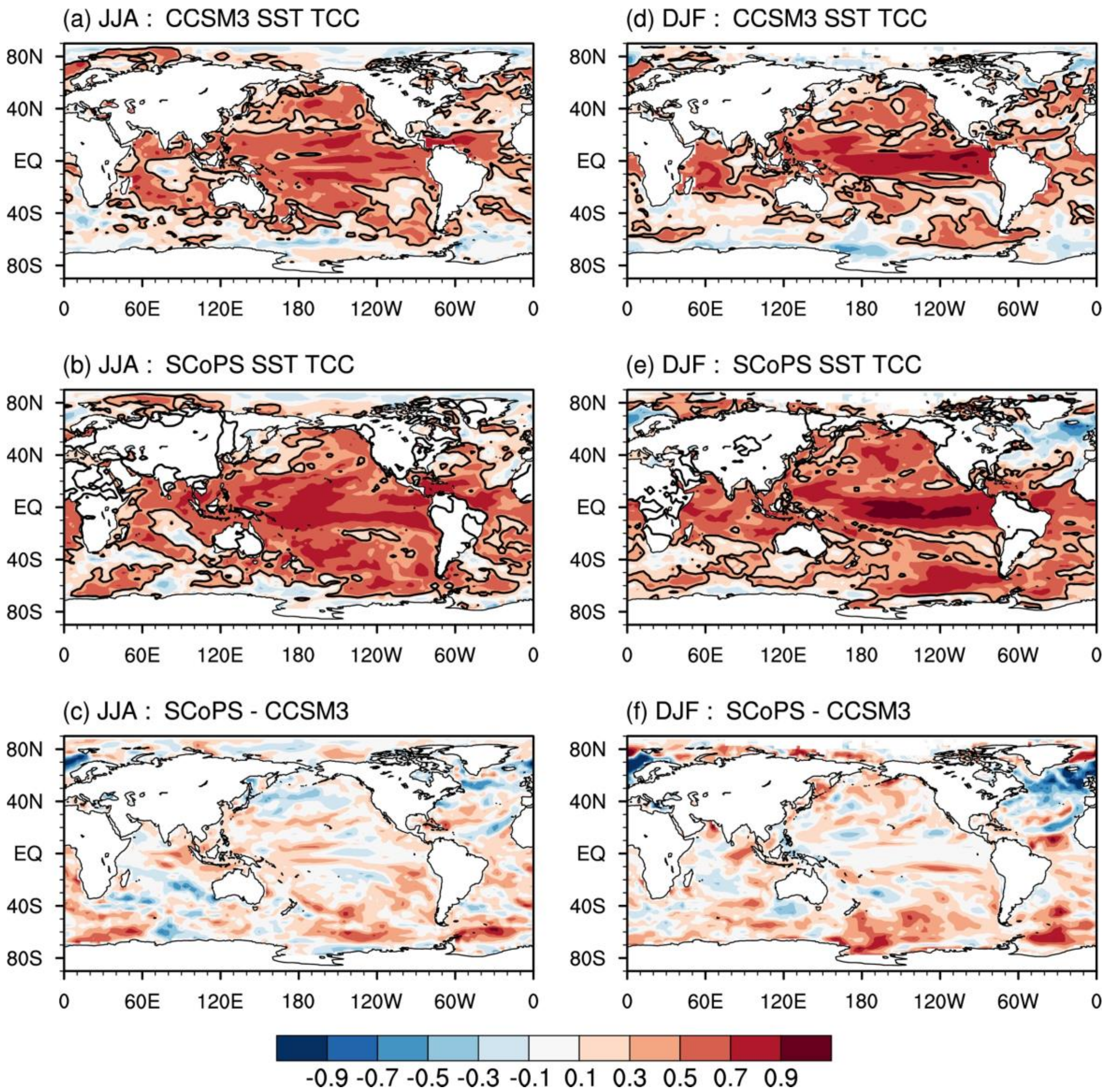

Fig. 3. Prediction skill of the sea surface temperature between observation and (a) CCSM3 for JJA and (b) SCoPS hindcast with 1-month lead 3-month mean hindcast for JJA. (c) The difference between (a) and (b). Prediction skill of the sea surface temperature between observation and (d) CCSM3 for DJF and (e) SCoPS hindcast with 1-month lead 3-month mean hindcast for DJF. (f) The difference between (d) and (e). Black thick lines in (a) to (e) indicates the area statistically significant at the 95% level.

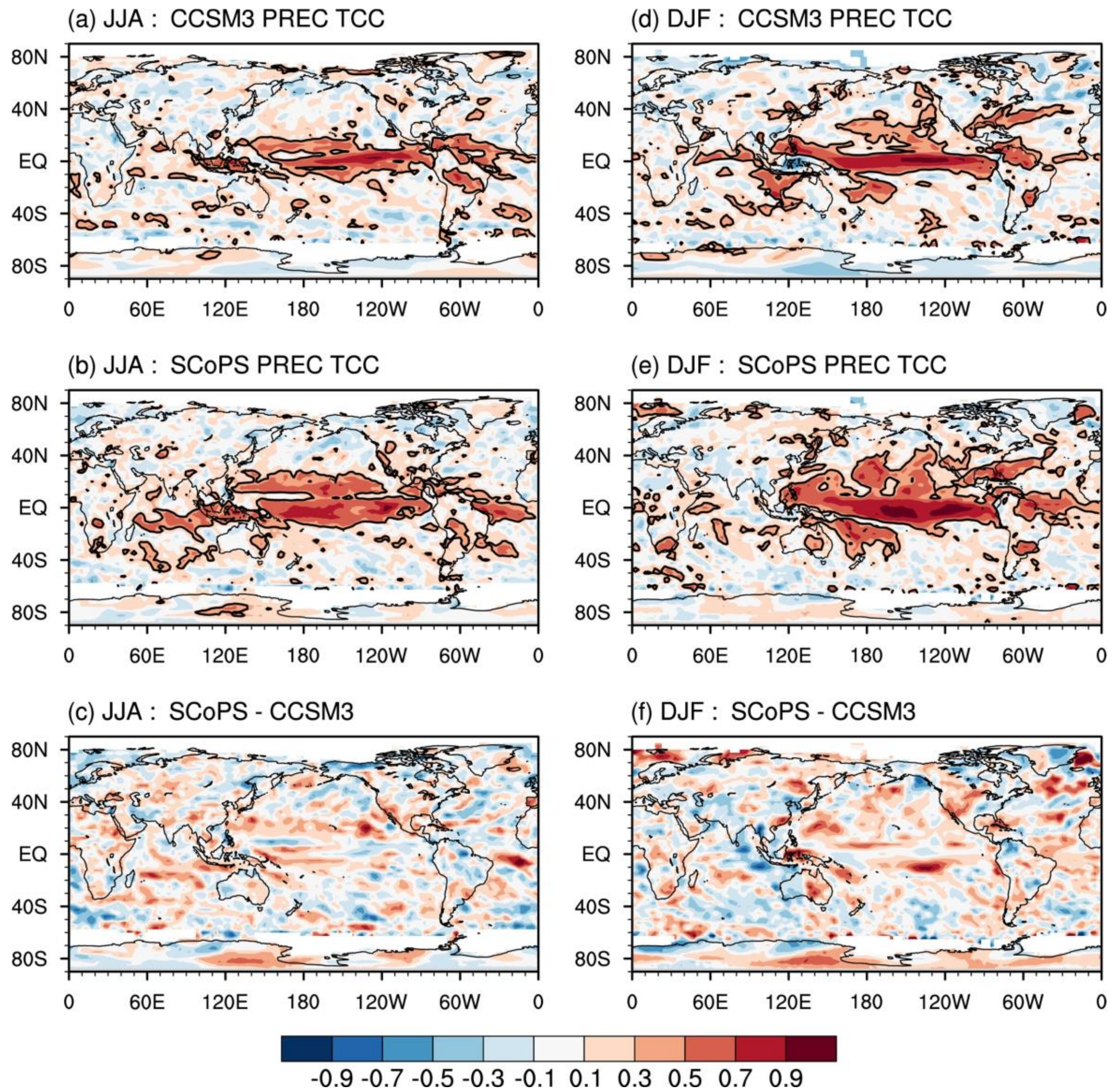

Fig. 4. Same as Fig. 3, but for precipitation.

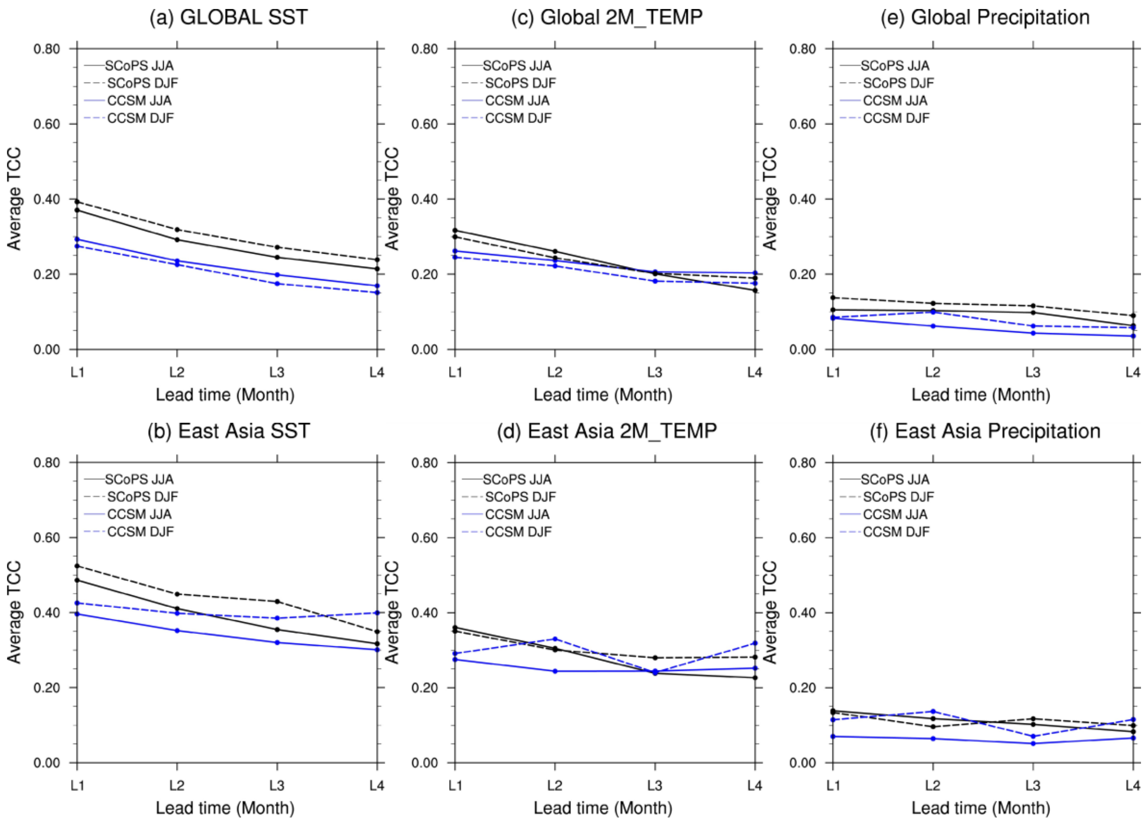

Fig. 5. Averaged TCC (a) for global SST, (b) East Asia SST, (c) global 2-m temperature, (d) East Asia 2-m temperature, (e) global precipitation, and (f) East Asia precipitation from CCSM3 (blue) and SCoPS (black) with 3-month mean hindcast for JJA and DJF.

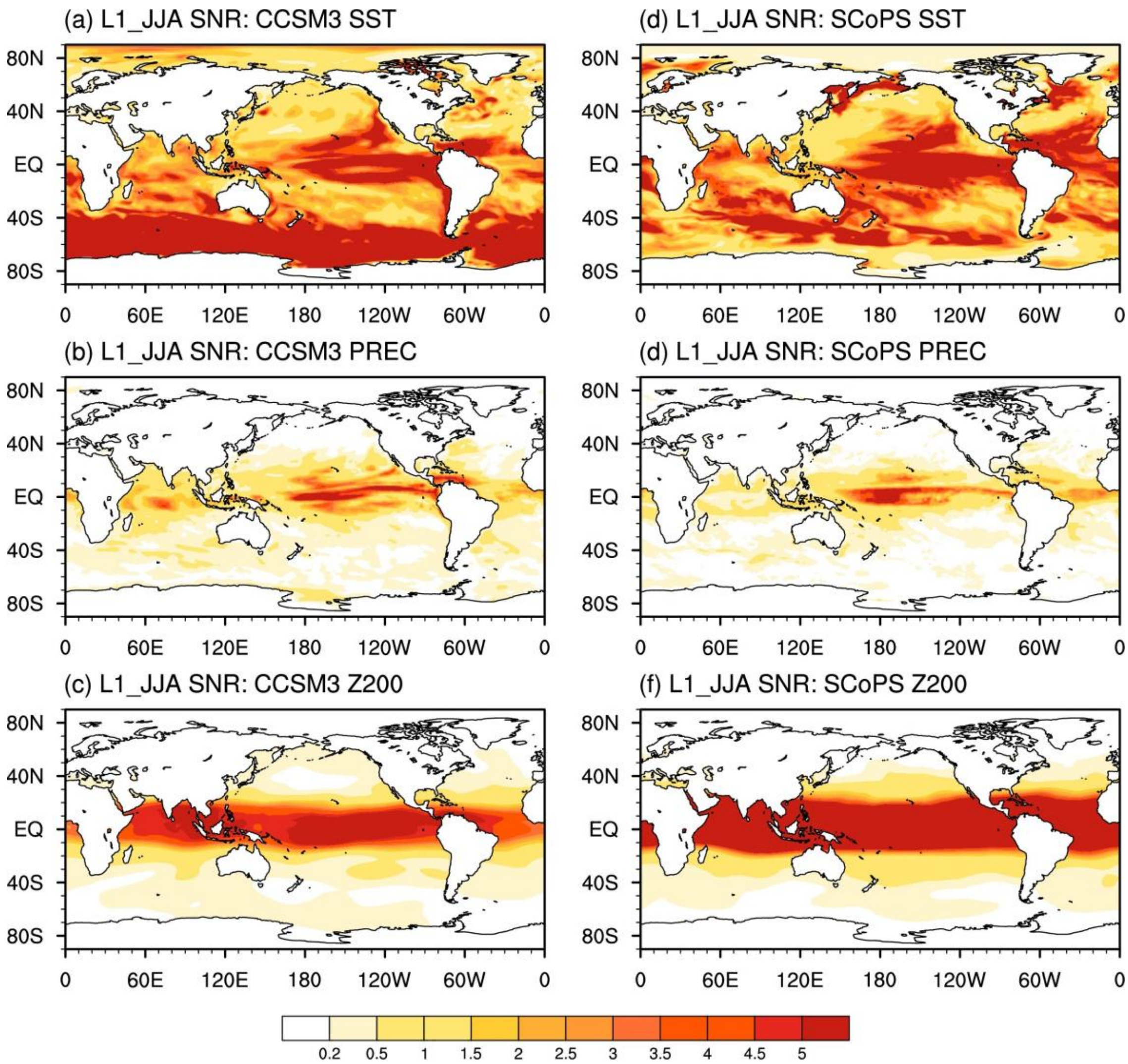

Fig. 6. Signal-to-Noise (SN) ratio for (a), (d) SSTs, (b), (d) rainfall, and (c), (f) 200 hPa geopotential heights from CCSM3 and SCoPS for 1-month lead time. The SN ratio is computed as the ratio of standard deviation of ensemble means, and standard deviation of individual forecasts from the ensemble mean forecast. Larger (small) SN ratio is indicative of higher (lower) predictability.

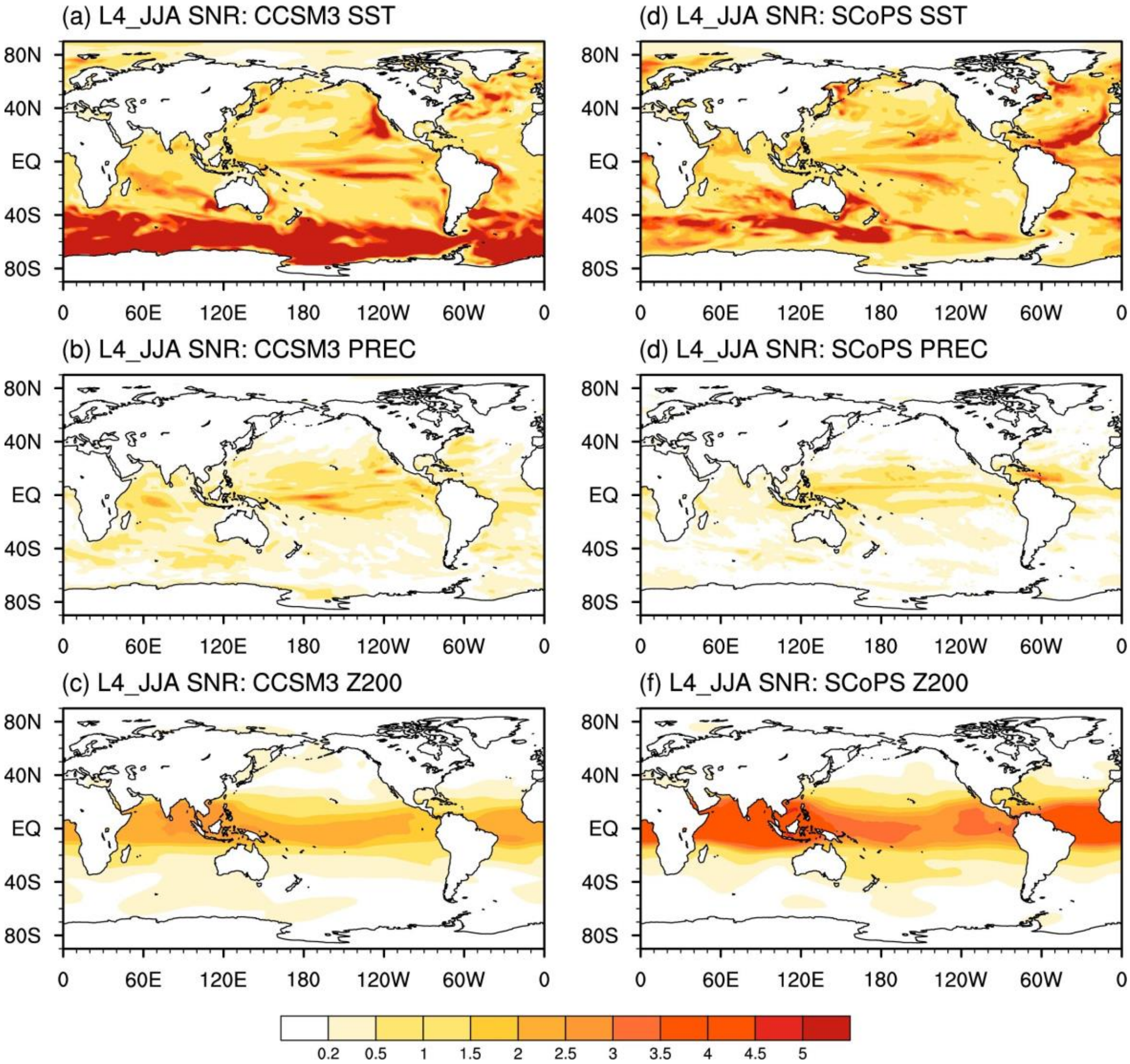

Fig. 7. Same as Fig. 6, but for 4-month lead time.

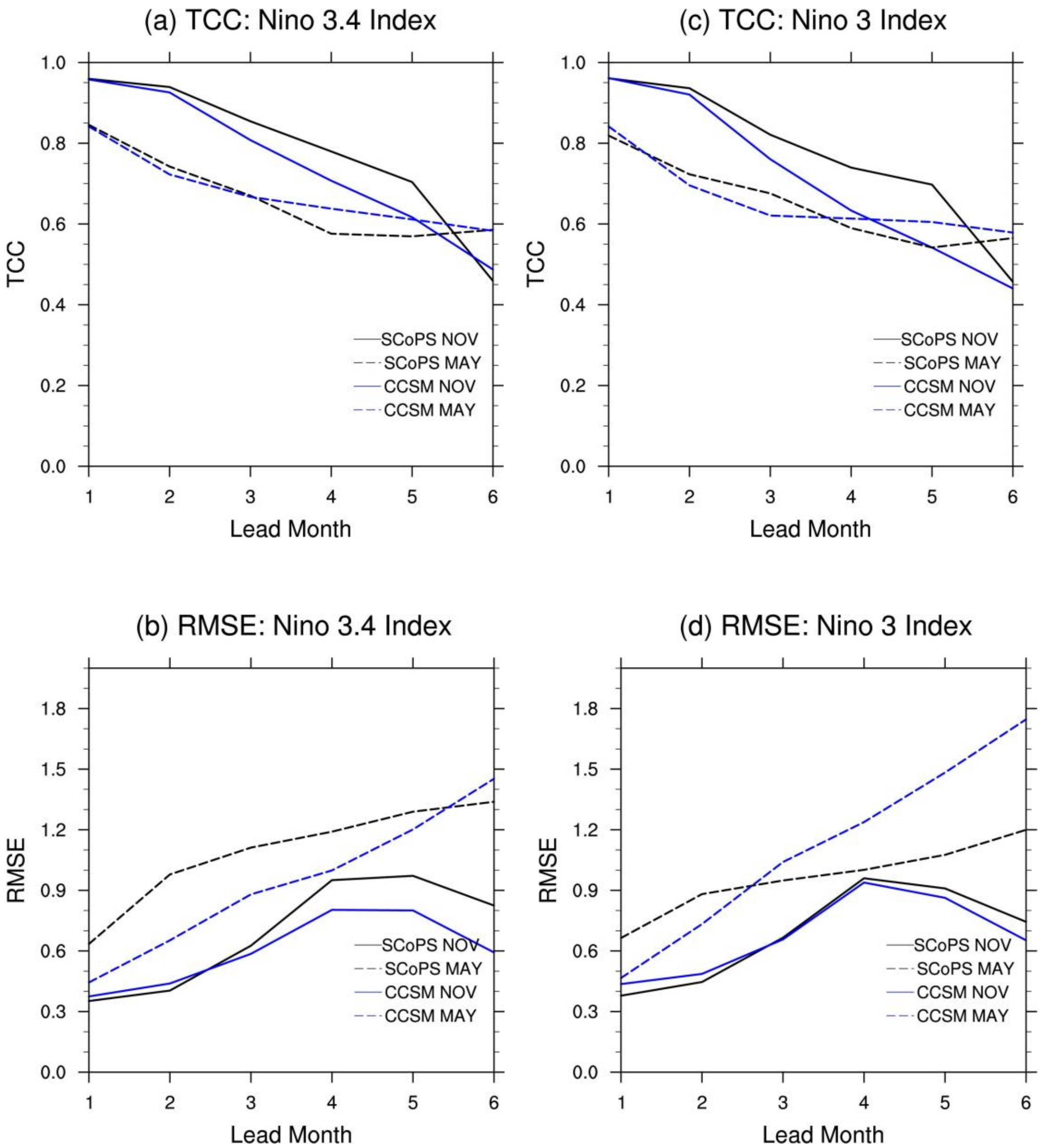

Fig. 8. (a) Temporal correlation coefficient of Niño 3.4 indices, (b) root mean square error of Niño 3.4 indices, (c) temporal correlation coefficient of Niño 3 indices, and (d) root mean square error of Niño 3 indices from CCSM3 (blue), SCoPS with May-initialized hindcast (black dashed lines), and SCoPS with November-initialized (black solid lines) hindcast.

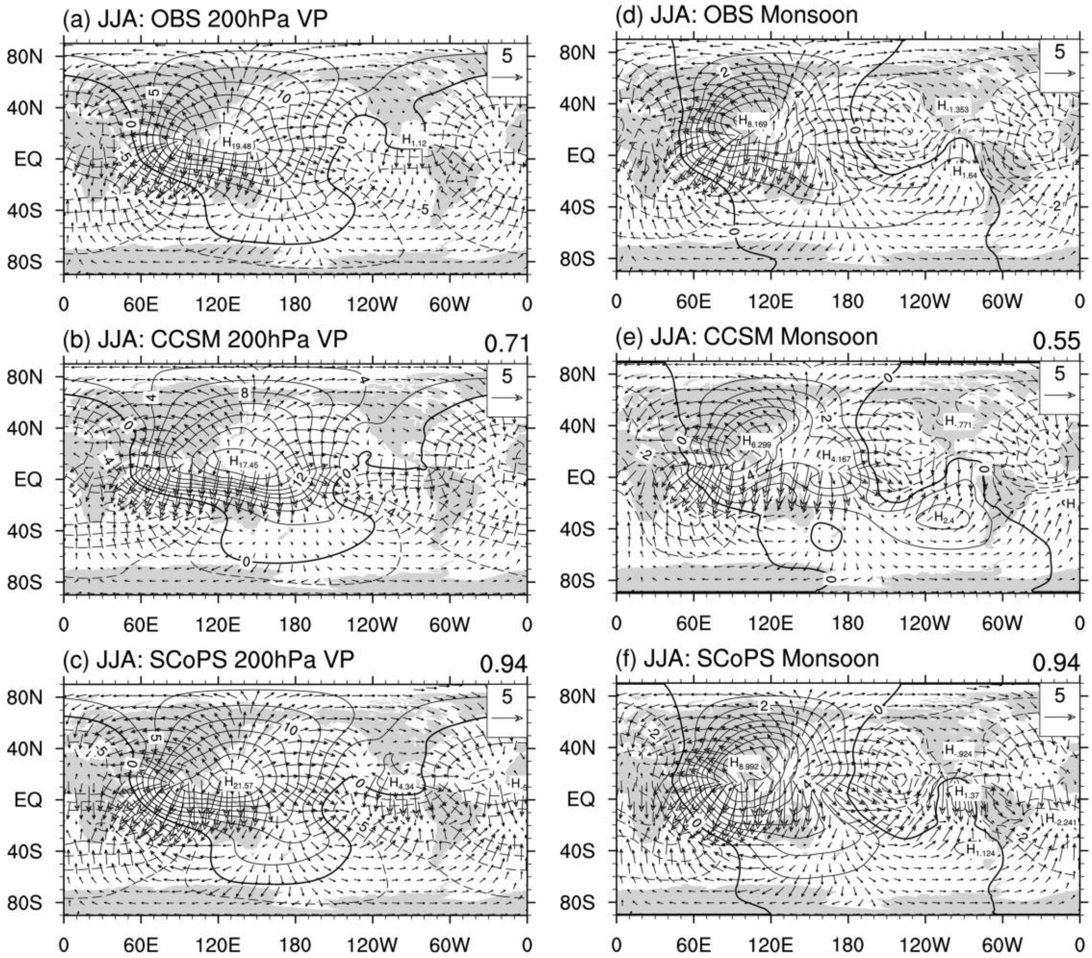

Fig. 9. Seasonal mean velocity potential and divergent wind at 200 hPa for the (a) reanalysis data, (b) CCSM3, and (c) SCoPS hindcast period (1982–2013) with 1-month lead time for JJA. The monsoon circulations, which are defined by the seasonal variation of the velocity potential are plotted with divergent wind for the (d) reanalysis data, (e) CCSM3, and (f) SCoPS hindcast. The units are 10^6 m^2 s^{-1}.

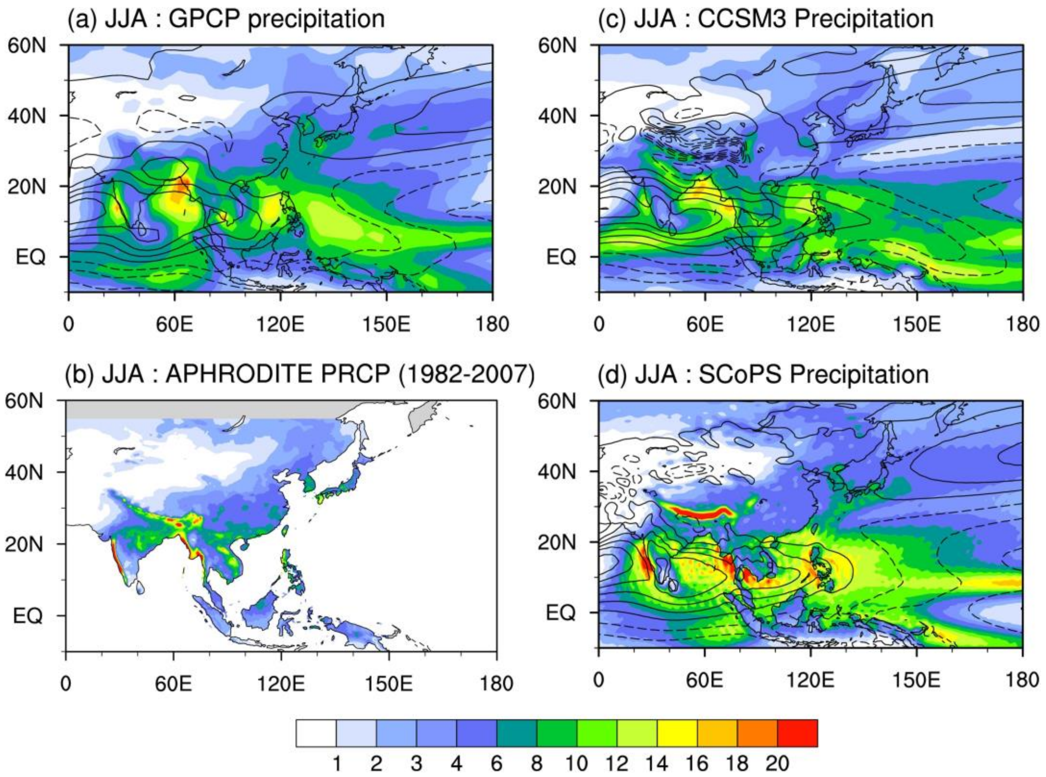

Fig. 10. Climatological mean precipitation (shaded) and zonal wind at 850 hPa (contour) from (a) GPCP and ERA-interim, (b) APHRODITE precipitation, (c) CCSM3, and (d) SCoPS during June to August, averaged over 32 years (1982–2013). Initial month for both hindcasts is May (1-month lead time).

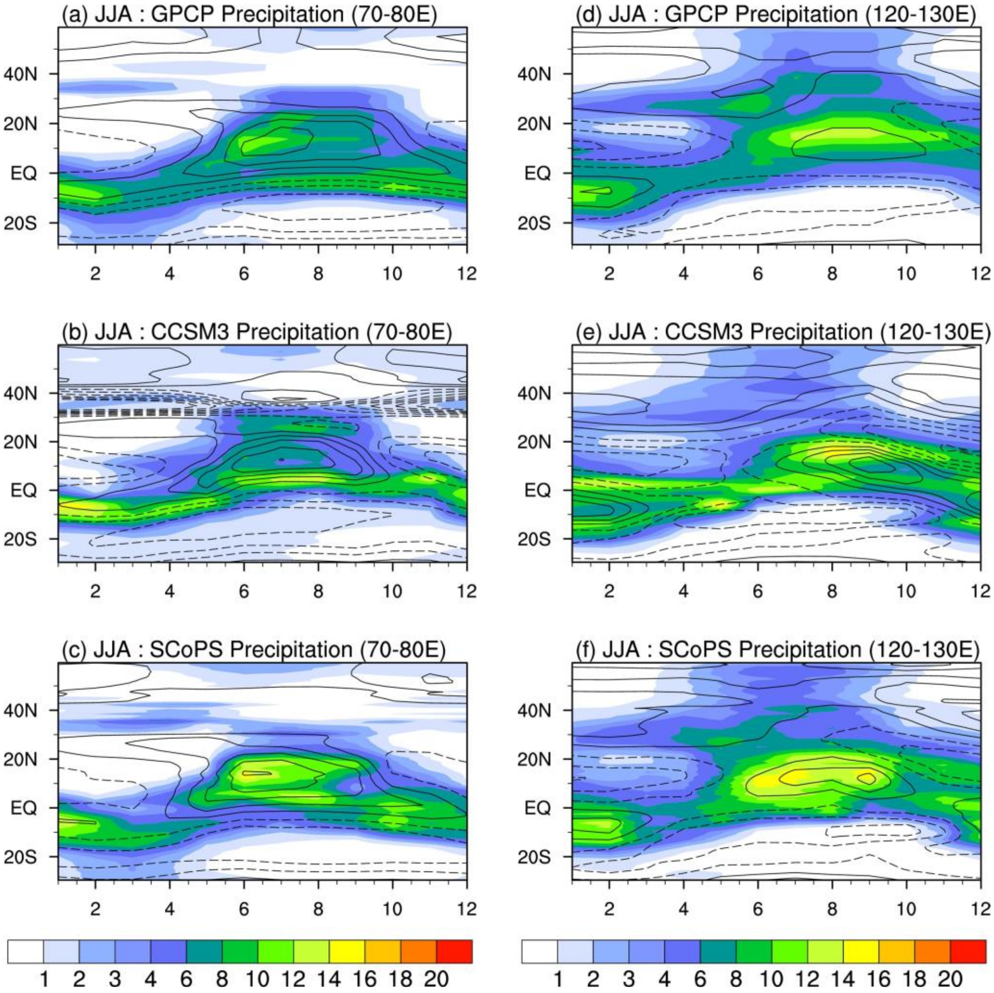

Fig. 11. Latitude-time cross section of climatological mean precipitation and 850-hPa zonal wind from (a) GPCP and ERA-interim over the Indian region (70–80 E°), (b) CCSM3 over the Indian region, (c) SCoPS over the Indian region, (d) GPCP and ERA-interim over the East Asian region (120–130 E°), (e) CCSM3 over the East Asian region, and (f) SCoPS over the East Asian region.

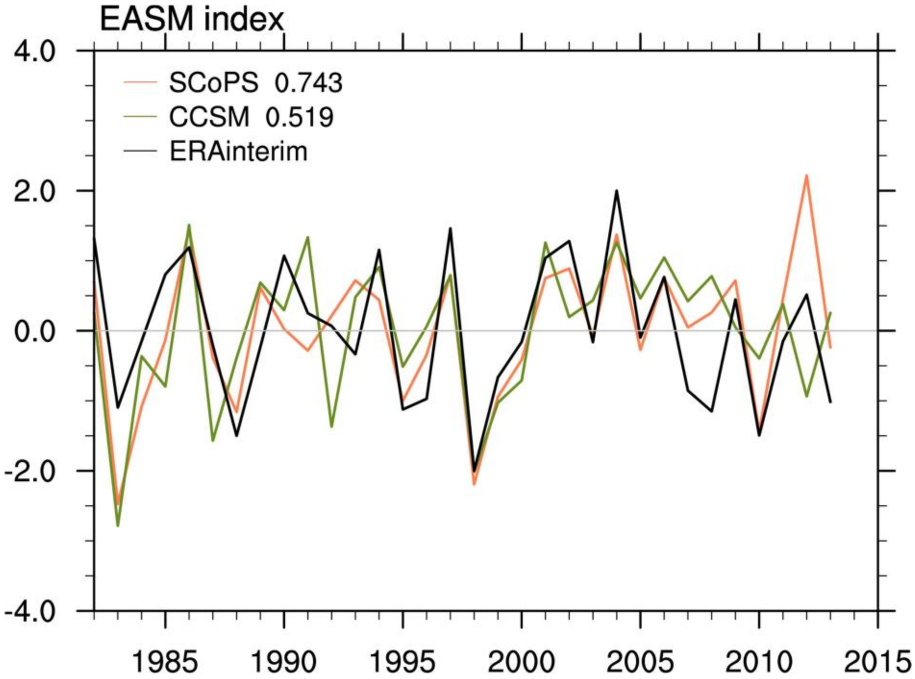

Fig. 12. The summer (JJA) EASM (East Asian Summer Monsoon) indices with correlation coefficients from reanalysis data, CCSM3, and SCoPS hindcasts. EASM is defined as the zonal wind anomaly at 850 hPa, averaged over the region of 5–10 °N and 130–150 °E minus that over 25–30 °N and 110–130 °E by Lee et al. (2014).

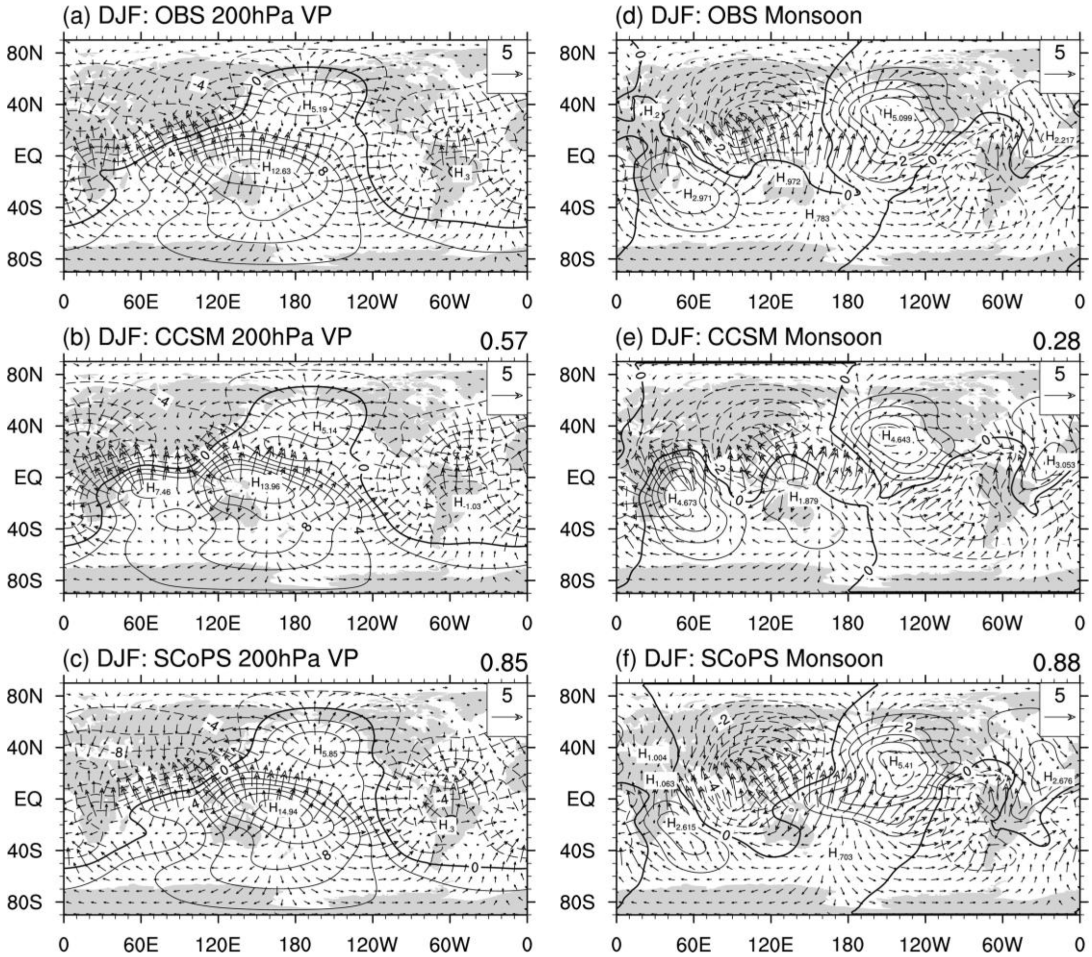

Fig. 13. Same as Fig. 9, but for hindcast with starting November.

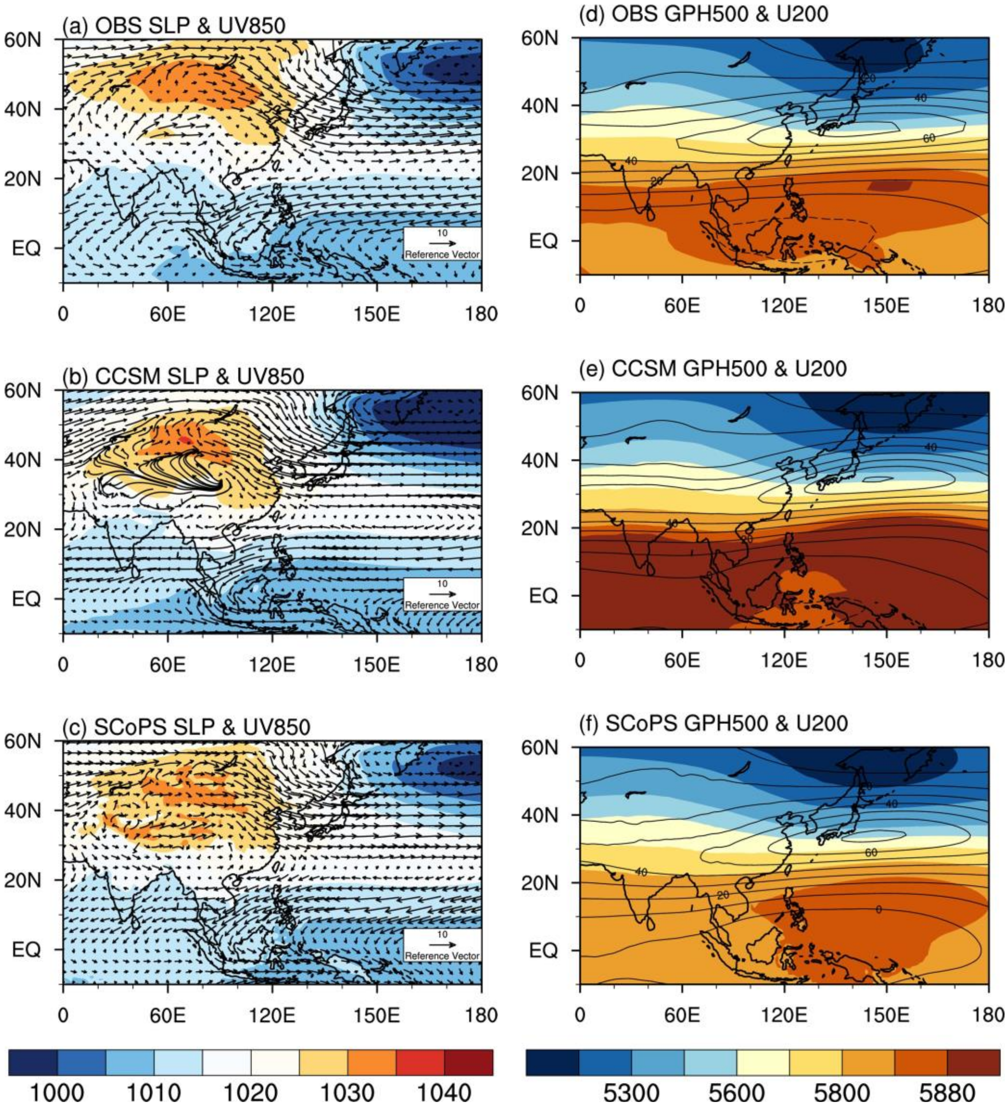

Fig. 14. Climatological mean sea level pressure (left; shaded), wind vector at 850 hPa (left; contour), geopotential height (right; shaded), and zonal wind at 200 hPa (right; contour) from reanalysis data (top), CCSM3 (middle), and SCoPS (bottom) during December to February, averaged over 32 years (1982–2013). Initial month for both hindcasts is November (1-month lead time).

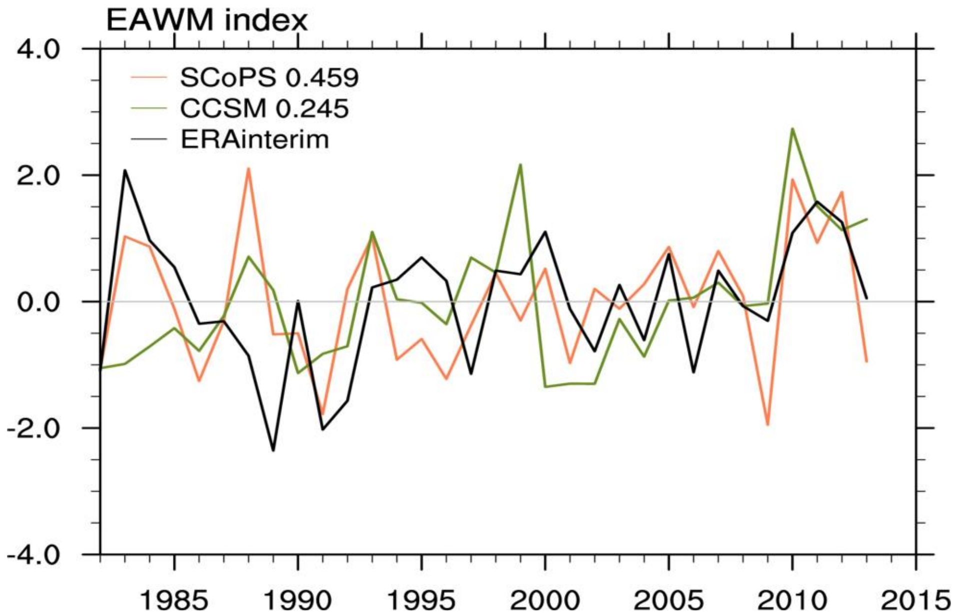

Fig. 15. Normalized EAWM indices from reanalysis (black), CCSM3 (olive), SCoPS (coral). EAWM is defined as the index from Li and Yang (2010).

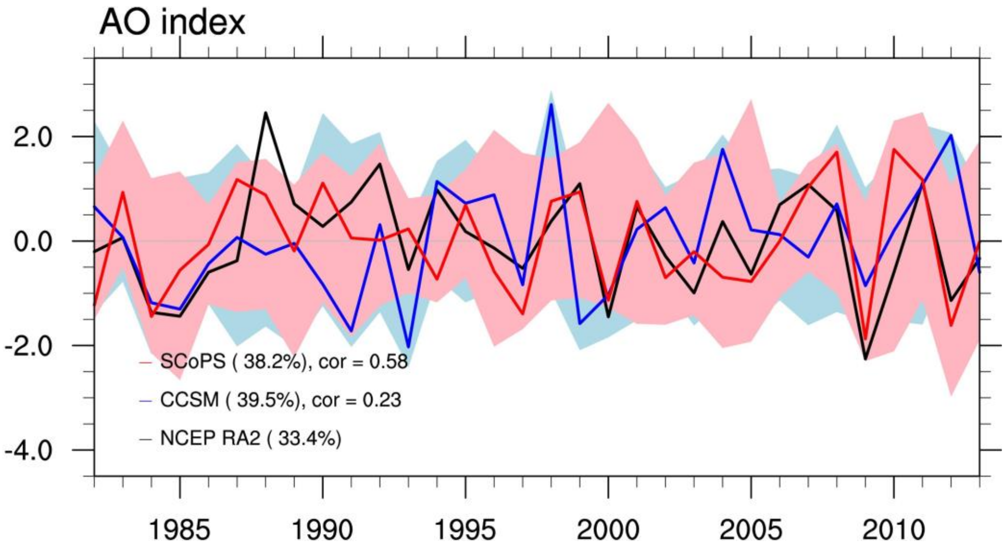

Fig. 16. Ensemble-averaged AO index from reanalysis (black), CCSM3 (blue), and SCoPS (red). Filled areas indicate the results from all ensemble simulation for CCSM3 (blue) and SCoPS (red). Percentages in left bottom string indicate explained variance (averaged explained variance from each ensemble member) from the pattern.

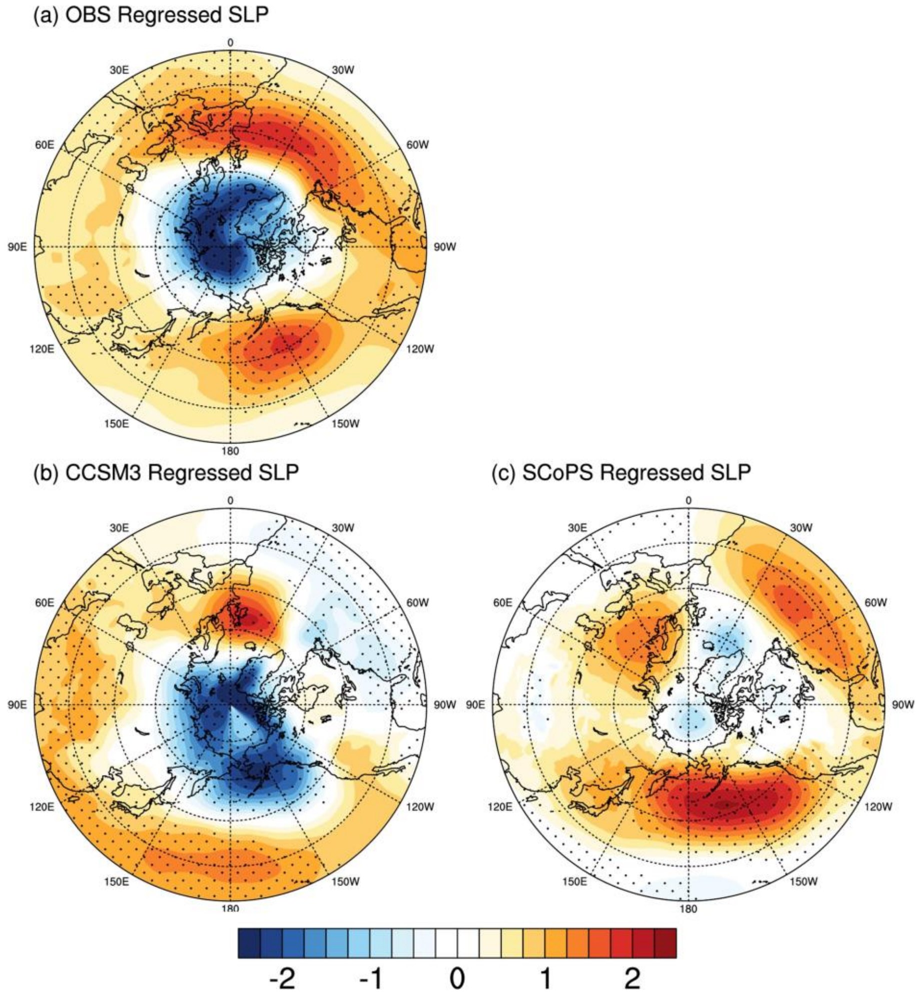

Fig. 17. DJF mean sea level pressure anomaly regressed onto the leading PC for 1982–2013 from (a) reanalysis data, (b) CCSM3, and (c) SCoPS simulations with 1-month lead time.